



WPI

Extracting Water from the Martian Environment

A Major Qualifying Project

Submitted to the Faculty of

WORCESTER POLYTECHNIC INSTITUTE

In partial fulfillment of the requirements for the Degree in Bachelor of Science

Submitted on April 28th, 2022, by

Lydia Ellen Tonani

Advisors: Professor Carrick Eggleston, Professor John Bergendahl, and Professor John Sullivan

This report represents the work of one or more WPI undergraduate students submitted to the faculty as evidence of completion of a degree requirement. WPI routinely publishes these reports on its website without editorial or peer review.

Abstract

For many years, space organizations have studied, planned, and prepared for a crewed mission to Mars. Although scientists have found water on Mars as frozen brine and water ice, the absence of an abundant potable water supply is a fundamental obstacle to crew survival. The Mars Phoenix Lander found evidence of permafrost only a few cm below the regolith surface and found that perchlorate was five times more abundant than chloride. Therefore, this project aimed to develop a water treatment method that converts frozen perchlorate brine into potable water. I selected progressive freeze concentration as the water purification method to achieve this goal and designed a prototype capable of sustaining the process in Mars's conditions. Experiments used a one-molal magnesium perchlorate starting solution, and all experiments successfully produced a treated product of reduced salt concentration along with a residual brine of elevated salt concentration.

Acknowledgements

I would like to thank my advisors, Professors Carrick Eggleston, John Bergendahl, and John Sullivan for their continued support, assistance, commitment, and guidance that were pivotal to the project's success. Thank you all very much for giving me this opportunity to expand my horizons and research abilities while pursuing this research topic.

I would also like to thank Professor Fiona Levey and Professor Sergey Makarov for helping me expand my understanding of the heat transfer, thermodynamic, and electrical processes involved in my hypothesis and prototype's development. I'm also grateful to Prototyping Specialist Mitra Varun Anand for their invaluable contributions to the prototype's development and am thankful for Higgins Laboratory Manager Peter Hefti and Environmental Engineering Laboratory Manager Donald Pellegrino for teaching me more about laboratory equipment and helping me obtain the resources necessary for my MQP. I would like to extend my gratitude to my colleague and Architecture graduate Marina Farias Schuttel for helping me learn how to navigate Rhinoceros 6 during the beginning of my project. Your guidance and patience allowed me to virtually design my prototype and better prepare for the project's building process.

I am also grateful to the Instruction Librarian Paige Neumann, STEM Instruction Librarian Albert Lin, and the Associate Director for Library Academic Strategies Lori Jean Ostapowicz-Critz for all their support, advice, and assistance during the Major Qualifying Project's research process. Your contributions were crucial components to the project's success. I would also like to thank Laboratory Technician James Loiselle and the Administrative Assistants Barbara Furhman, Joan Langlois, and Cynthia Bergeron for their contributions during

the project's prototyping stage. Without your help, I would not have been able to obtain all the materials necessary for the project's completion.

Last, but certainly not least, I would like to extend my gratitude to my family, friends, and significant other for all their encouragement and care during this project experience. Your heartening words and emotional support throughout my research have been indispensable to the project's success and my academic journey.

Statement on Design

This project's primary objective was to develop a water treatment method that could convert frozen perchlorate brine into potable water. After selecting progressive freeze concentration as the water treatment method investigated in this study, I evaluated the viability of the process to provide a potable water supply for astronauts on Mars. With this objective in mind, I considered the economic, environmental, social, political, ethical, health, safety, constructability, and sustainability factors involved in the prototype and in freeze crystallization in an extraterrestrial environment.

When selecting the prototype's materials and electronic components, I considered the cost-effectiveness of the insulation and the treatment station's composition alongside their ability to fulfill their purposes within the project. An example of this occurrence is that, although I could have chosen polyurethane foam as the insulation material, polystyrene foam has a similar thermal conductivity, a higher thermal resistance rating, and can be found at lower prices on the market. Moreover, I utilized the open-source software Arduino, the Arduino Uno R3 microcontrollers, and the Thermocouple Amplifier MAX31855 Breakout Boards due to their cost-effectiveness and user-friendliness. I also utilized the resources available to me at the Worcester Polytechnic Institute when determining the project's data collection methods, such as the Model 150 Orion Conductivity Meter, further increasing the project's cost-effectiveness. The economic design factors and the materials' list are discussed further in Sections 3.1., 3.2.1. and 3.2.2. within this report.

Since the project will be applied primarily in the Martian environment, it will not impact Earth's natural environments. However, regular safety inspections and environmental barriers must be fulfilled while the prototype is on Mars to avoid contaminating Mars's regolith via

structural failures such as leaks. The environmental barriers could be walls capable of withstanding the pressure differential between the astronauts' habitation and the Martian atmosphere and thoroughly separate the outside environment from the prototype and the solutions within it before, during, and after the progressive freeze concentration occurs.

This project proposes a water treatment method and water treatment system that has the potential to further human knowledge regarding the solar system and the history of its planets by granting astronauts an initial water supply on Mars and a means to replenish the crew's water losses. Thus, the implementation of the prototype and the ideas discussed in this report can facilitate social progress by providing the resources necessary for new pathways to scientific advancement in space exploration.

Furthermore, this project abided by the American Society of Mechanical Engineers Code of Ethics to preserve the safety, health, and well-being of the public and the subjects that will benefit from the prototype's effects. I also strived to develop new opportunities for further research through my work, respected the intellectual and proprietary information of the researchers cited in this paper, avoided conflicts of interest throughout my study by conducting honest and impartial research, and aspired to increase the renown of my field of study through my work [1].

I aimed to safeguard the health and safety of the public and the astronauts involved in future crewed missions to Mars by proposing processes that grant astronauts an initial water supply on Mars, and a means to replenish the crew's water losses. In sections 4, 5, and 6 of this paper, I discussed the experimental and design recommendations that should be implemented in future research to increase the purity of the resulting aqueous solutions so the astronauts on the

future missions to Mars can consume potable water and continue their missions with optimal health.

Throughout the design process, I selected materials that could be transported to Mars given the weight and volume constraints on such a mission. The experimentation procedure and the materials selected for the prototype are discussed further in Sections 3.1., 3.3., 3.3.1., 3.3.2., 3.2.3., and 3.2.4., while the prototype's dimensions are disclosed in Appendix II. Even though the prototype's design primarily served to test if progressive freeze concentration could be utilized to purify perchlorate brine on Mars, the model's dimensions and design can be altered to maintain the temperature differential, enable process automation, purify the amount of water needed to sustain the crew, and permanently include the temperature, pressure, and electrical conductivity reading devices. A notable example of this change is that, since Mars's atmospheric temperature closely resembles the sublimation temperature of dry ice, an ice box will not be needed to maintain the temperature differential for the progressive freeze concentration to occur; the process makes use of the Martian environment. My recommendations for modifications used in future experiments and versions of this prototype for use on Mars are written in Section 5 of this report.

This project is intended to suggest an initial water source for the astronauts on future missions to Mars and to supply the crew's daily water losses. However, to preserve the Martian environment and its unique properties, it is encouraged that other means of water purification and reclaiming are developed over the course of subsequent missions to the red planet.

Statement on Professional Licensure

The National Council of Examiners for Engineering and Surveying (NCEES) regulates the practice of engineering throughout the United States through the use of professional licensure for proficient engineers. This process allows American states to ensure that the engineers practicing in their territories are competent in their field, ensure safety and productivity within the workplace, and have the knowledge and experience to benefit their communities through their work. The licensure process in the United States occurs through the use of accredited education, experience, and exams.

The process begins when an individual pursues a Bachelor's degree in Engineering at an ABET-accredited institution, where the student will obtain technical and practical knowledge in their engineering field of choice. Once the student graduates or is in their last semester of study at a university, they must take the first exam required to become a professional engineer: the Fundamentals of Engineering (FE) exam, which is also known as the Engineering in Training (EIT) exam.

After the candidate passes the FE exam and becomes a certified Engineer in Training, the individual must obtain four years of experience in the engineering industry while working under the supervision of a certified Professional Engineer before completing the final step required for professional engineering licensure: passing the Professional Engineering (PE) exam. Although the professional engineering licensure process can be rigorous, becoming a certified Professional Engineer can grant individuals numerous career opportunities within their fields. Moreover, there are specific tasks within the engineering industry that only Professional Engineers can execute, such as developing engineering plans and approving designs and other indispensable documents while upholding workplace and public safety.

Throughout this project, I was advised by licensed engineers who have invaluable experience and knowledge in their fields of study. By learning more about the professional licensure process and its importance during my research, I gained a greater appreciation for the role that professional licensure has in verifying that engineers produce quality work while ensuring safety and productivity. When utilizing the designs within this paper in the future, additional consultation with certified Professional Engineers may be necessary.

Statement on the Major Qualifying Project's Broader Impacts

This project proposes a water treatment method and water treatment system that has the potential to further human knowledge regarding the solar system and the history of its planets by granting astronauts an initial water supply on Mars and a means to replenish the crew's water losses. Thus, the implementation of the prototype and the ideas discussed in this report can facilitate social progress by providing the resources necessary for new pathways to scientific advancement in space exploration.

Furthermore, this project abided by the American Society of Mechanical Engineers Code of Ethics to preserve the safety, health, and well-being of the public and the subjects that will benefit from the prototype's effects. I also strived to develop new opportunities for further research through my work, respected the intellectual and proprietary information of the researchers cited in this paper, avoided conflicts of interest throughout my study by conducting honest and impartial research, and aspired to increase the renown of my field of study through my work [1].

Finally, I aimed to propose a water treatment method that would be cost-effective and profitable to the businesses that decide to expand on the current prototype's model. The materials I selected during the design and building process are widely available and inexpensive, and the software I utilized to collect my thermal data are all open-sourced. In addition, the solutes extracted from the decantation, filtration, and progressive freeze concentration proposed in Section 5 can be refined and reused to manufacture products that will be useful in future space missions. An example of this is how perchlorate can be used to create rocket propellant for future missions to Mars or power the Mars Ascent Vehicle required to return to Earth [9]. Thus, this project's broader impacts have the potential to benefit society and businesses while being ethical

and safeguarding the well-being of the public and of the astronauts that will directly benefit from the model's implementation.

Table of Contents

Abstract	i
Acknowledgements	ii
Statement on Design	iv
Statement on Professional Licensure	vii
Statement on the Major Qualifying Project’s Broader Impacts	ix
Table of Contents	xi
Table of Figures	xiii
1. Introduction	1
2. Background.....	3
2.1. Potential Missions Sites for Crewed Missions	3
2.2. Water Presence on Mars and Subsurface Glacier Observations	5
2.3. Potential Uses for Perchlorate Compounds after Water Purification.....	8
2.4. Daily Astronaut Water Needs and Subsurface Glacier Assumptions	9
2.5. Analysis of Water Purification Methods for the Prototype.....	10
2.5.1. Sublimation	11
2.5.2. Forward Osmosis and Reverse Osmosis.....	13
2.5.3. Freeze Crystallization and Progressive Freeze Concentration.....	16
3. Methodology.....	19
3.1. Materials.....	19
3.2. Prototype’s Design	20
3.2.1. Materials Science and Stress Analysis	22
3.2.2. Heat Transfer and Thermodynamics	24
3.3. Experimentation Procedure	26
3.3.1. Prototype Testing	27
3.3.2. Freezing Rate Testing	28
3.3.3. Successive Testing	29
3.3.4. Electrical Conductivity Reading	29
4. Results	31
5. Discussion.....	40
5.1. Sources of Error	40
5.2. Recommendations for Future Research and Prototype Iterations	41

6. Conclusions	43
References	44
Appendix I: The Prototype's First Iteration.....	52
Appendix II: The Prototype's Final Iteration.....	55
Appendix III: Experimental Data involving Temperature over Time	57
Appendix IV: Experimental Data regarding the Solution's Molality over Cooling Rate.....	60
Appendix V: Standard Deviation Calculations.....	64

Table of Figures

Figure 1	7
Figure 2	10
Figure 3	12
Figure 4	12
Figure 5	14
Figure 6	14
Figure 7	15
Figure 8	18
Figure 9	20
Figure 10	21
Figure 11	23
Figure 12	28
Figure 13	30
Figure 14	31
Figure 15	32
Figure 16	33
Figure 17	34
Figure 18	35
Figure 19	36
Figure 20	36
Figure 21	37
Figure 22	37
Figure 23	38
Figure 24	52
Figure 25	53
Figure 26	53
Figure 27	55
Figure 28	55
Figure 29	56

1. Introduction

For many years, space organizations around the globe have studied, planned, and prepared for a crewed mission on Mars. The National Aeronautics and Space Administration (NASA) has conducted numerous investigative missions to understand the red planet, including the use of space rovers [2], conceptual design studies [3,4], and chemical analyses of Martian regolith samples [5,6]. Furthermore, many companies such as SpaceX and Lockheed Martin have been developing Martian settlement plans [6] and designs for vehicles that can transport astronauts to Mars [7,8]. Nevertheless, even though numerous organizations are preparing prototypes and contingency plans for future human missions to Mars, there are still many questions that scientists must answer for this goal to become a reality, such as the expedition site's altitude, elevation, and potential resources for the mission [9]. However, all the known potential water sources for future human habitations on Mars exist in frozen brine and water ice either in the Martian subsurface in the mid-latitudes [9,10] as brine or in the planet's poles [14,17] and are likely contaminated by perchlorate and other soluble salts [18,21,22] distributed consistently throughout the Martian landscape [5]. Therefore, determining the astronauts' water supply will be a crucial component of the success of a crewed mission to Mars.

To provide an initial water source for the future crewmembers on Mars and satisfy the degree requirements for the Bachelor of Science in Mechanical Engineering and Environmental Engineering, this Major Qualifying Project (MQP) aimed to develop a water treatment method that converts frozen perchlorate brine into potable water. To achieve this goal, the project had two research objectives:

1. identify the chemical separation techniques that will occur within the treatment system to obtain potable drinking water, and

2. design, build, and test a prototype that applies the treatment methodology

In this paper, I outlined potential mission sites on Mars with water resources, discussed potential processes that can desalinate the melted brine ice, and developed a prototype that can purify the subsurface ice to ensure a water source for future astronauts on Mars.

2. Background

2.1. Potential Missions Sites for Crewed Missions

When planning space missions and preparing the equipment and transportation required, scientists carefully consider the expedition site's altitude, elevation, and potential resources to ensure that the location is propitious for a landing system to function adequately and for surface operations to occur [9]. The places on Mars that satisfy these criteria are in lower to mid-latitudes [9,10], have ice resources [9], lower elevations [9], and have higher insolation and temperatures [9]. After considering these criteria, four locations on Mars were selected that demonstrated promise for human missions: Hellas Planitia, Arcadia Planitia, Utopia Planitia, and Vastitas Borealis.

Hellas Planitia is an impact crater that is 3000 km long and 1500 km wide in the mid-latitudes of Mars at 42.43 degrees South and 70.5 degrees East [11,12]. The basin has an atmospheric pressure of 1155 Pa, which is 89% higher than the planet's average pressure (610 Pa) and above the triple point of water [13]. The location also exhibits minerals correlated to the presence of liquid water, such as sulfates (in the form of gypsum), carbonates, oxides, and phyllosilicates [11]. The crater also exhibits the terrain characteristics of glacier-like formations (GLFs), including polygonized terrain, linear terrain, and rectangular-ridge terrain, which comprise approximately 25%, 22%, and 7% of the GLF's surface area, respectively [13]. Thus, this potential site has many mineral and physical properties that can indicate the occurrence of water in solid and liquid form, which, when combined with its latitude and regional topography, makes the Hellas basin a point of interest for missions to Mars.

In contrast with the Hellas basin, Arcadia Planitia is a Martian region replete with flat-lying plains located between 37 and 43 degrees North and 193 and 204 degrees East. The area

also presents polygonized terrain indicating ground ice sublimation and cryoturbation and a high consistency for subsurface water-ice with an extensive layer spanning a $1.2 \times 10^6 \text{ km}^2$ area of the plains according to Subsurface Water Ice Mapping (SWIM) [14]. Moreover, Morgan et al. found the ice in Arcadia Planitia due to radar surface analysis and lower power returns from ~5 meters deep into the regolith, which indicates that a thin layer of debris (less than 2 meters thick) is covering the glacial ice or that it is covered in a meters-thick layer of highly porous material [9]. In light of this information, it is clear that Arcadia Planitia's topography, available resources, and insolation make it a promising location for future human missions on Mars.

Utopia Planitia is a region within Mars's northern plains, with a mid-latitude area between 38 and 47 degrees North and centered at 90 East degrees [10]. This location presents 100-meter-diameter thermal contraction polygons, mantled deposits, and thermokarst, which Séjourné et al. interpreted to be a "degraded ice-rich permafrost" and "a deposit of 80 m in thickness containing excess ice (~50–85% by volume) with a crater retention age of about 10 Ma" [15]. Since this region was also the Viking 2 Lander and the Zhurong Mars Rover sites [16], it is a feasible location for landing systems involved in crewed missions.

The final site analyzed in the background research was Vastitas Borealis, a large lowland region centered at 87.73 degrees North and 32.23 degrees East [17]. In that region, "ice has persisted continuously at a shallow depth for millions of years," and its terrain presents small polygons along with well-developed troughs [16]. Similar to Utopia Planitia, this location was already chosen as the mission site for the Phoenix Mars Lander. During the Phoenix Lander's surface operations, NASA collected and analyzed Martian regolith samples to determine the site's regolith chemical composition and obtain more information about Mars's surface. According to Toner et al.'s reanalysis of the data from the space probe, the most probable

abundant substances within the locations' samples were hydrated salts, including magnesium sulfate in the form of meridianiite, magnesium carbonate, magnesium perchlorate, sodium perchlorate, potassium perchlorate, sodium chloride, and calcium carbonate in the form of calcite. If chlorate ions are considered along with the previous model's predictions, sodium chlorate will precipitate instead of sodium perchlorate, and magnesium chlorate will be found alongside the magnesium perchlorate precipitates [18].

This chemical composition data aligns with observations from the samples collected by the Curiosity rover, which highlighted the presence of oxychloride compounds (such as perchlorates and chlorates) correlates as being the source of the oxygen and chlorinated volatiles in the mixture, and also observed H_2O releases consistent with H_2O bound to amorphous phases. These findings include water bound to aluminosilicate materials, ferric oxides, and oxyhydroxides, along with water present within an interlayer of phyllosilicates and H_2O from the dehydration of multiple salts and ferric oxyhydroxides. Leshin et al. also noted that chlorine had been observed in every soil analyzed on Mars, supporting the hypotheses that perchlorates are distributed throughout the planet's regolith and that the composition of Martian surface fines is "relatively constant at widely spread locations across the planet" [5].

2.2. Water Presence on Mars and Subsurface Glacier Observations

Unlike the perchlorate distribution, liquid water is rarely evident throughout the Martian surface. However, the temperatures within the low to mid-latitudes of Mars, along with the presence of perchlorate and chlorate salts, could form brines in the upper subsurface at cryogenic temperatures. The perchlorate and chlorate would subsequently percolate downward and refreeze to create an impermeable layer. Over time, this process can cause frozen and liquid brine, pure water ice, and liquid water to occur in the shallow subsurface of Mars, with a thin layer of

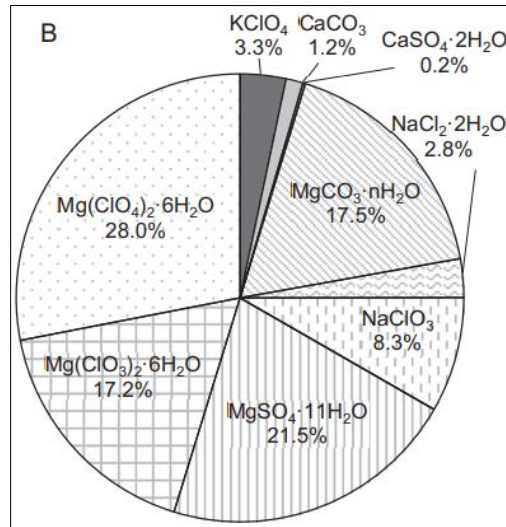
regolith acting as a barrier against the liquid and the ice's sublimation [19]. Chevrier et al. also observed that brines, regardless of their composition, are more stable within the subsurface of equatorial regions with lower water activity, which mirrors the trends present in the higher Martian latitudes [20]. Considering the resemblance of the thermodynamic trends and presence of frozen brine deposits in the Martian surface at higher latitudes and the subsurface at the low to mid-latitudes, along with the composition of the planet's surface, I will assume that the chemical properties of the Martian subsurface at the low to mid-latitudes is like that of the higher Martian latitudes in locations such as Vastitas Borealis.

Moreover, Boisson et al. addressed ambiguities found in the shallow subsurface radar (SHARAD) frequency data collected from Deuteronilus Mensae (situated within the Martian mid-latitudes) and Amazonis Planitia (located within lower Martian latitudes) by comparing the empirical evidence and geological phenomena on the red planet to analogous temperate permafrost in Fairbanks, Alaska. The researchers used resistivity and multiple-frequency ground-penetrating radar information from the Earth analog to find that Deuteronilus Mensae's lobate debris aprons could be more ice-rich than scientists initially believed. Boisson et al.'s results align with the hypothesis that the lobate debris aprons in the region are "residues of a much larger glacier protected from sublimation by a thin layer of debris" [21], indicating that the ice content of the geological formations could be higher than 80% [21]. Sori and Bramson also used a similar composition parameter, 80% water ice/20% dust and pure water ice, when calculating the temperature-depth profiles required for basal ice to melt at the south poles in current Martian conditions [22]. Considering Boisson et al.'s findings and Sori and Bramson's composition parameters, along with Chevrier et al.'s proposed brine stability model, I can assume that there are locations within the Martian subsurface at the low to mid-latitudes that possess a 4:1 water

ice to regolith dust ratio and a soil composition similar to that observed by Toner et al. (see Figure 1) [18]. This information will be utilized when designing the prototype and the analog samples for laboratory experimentation.

Figure 1

“The average proportion of salt phases by weight in Rosy Red inferred from the chemical divide model assuming that the ClO_3^- concentration is the same as the ClO_4^- concentration in the initial solution [18]”



Although scientists have found water present on Mars in the form of frozen brine deposits, the absence of an abundant, potable water supply is still an obstacle to a space crew’s survival on the red planet due to the presence of chemicals that are toxic to humans, such as perchlorates, chlorates, and sulfates. According to the United States Environmental Protection Agency (EPA), substances containing perchlorate are “readily absorbed through oral exposure and can migrate from the stomach and intestines to the bloodstream” and “can interfere with the iodide uptake into the thyroid gland at high enough exposures, disrupting the functions of the thyroid and potentially leading to a reduction in the production of thyroid hormones” [23].

Exposure to high doses of perchlorate can also cause a decrease in body weight and the gene expression of thyroglobulin and thyroperoxidase, along with hypertrophy of the thyroid gland [23]. In addition, compounds comprised of chlorate ions can also affect the thyroid gland by inhibiting its ability to uptake iodide [24]. Nevertheless, unlike the previously mentioned ions, water containing sulfate ions can have laxative effects on humans if exceeding 1,200 mg/L, but that correlation is not definitive in all the studies mentioned in the EPA's *Drinking Water Analysis Advisory* [25].

From this information, I concluded that the project's final prototype must be able to remove significant amounts of perchlorate compounds from the frozen brine deposits extracted from the Martian subsurface. With the regolith composition data from Toner et al., the three compounds containing perchlorate ions that must be addressed are magnesium perchlorate, sodium perchlorate, and potassium perchlorate [18]. Nevertheless, due to the relative insolubility of potassium perchlorate in water [18,26] and the weight percentage abundance of each compound within the Martian regolith, magnesium perchlorate becomes the primary soluble compound that will be separated from the water ice in the treatment station.

2.3. Potential Uses for Perchlorate Compounds after Water Purification

Once the magnesium and potassium perchlorate are removed, they can be used to create rocket propellant for use on Mars or augmenting the fuel required for the Mars Ascent Vehicle return to Earth [9]. For the propellant's combustion reaction to occur, the perchlorate would have to be combined with a potent fuel, such as in the case of ammonium perchlorate-based composite fuels [27]. In-situ resource utilization could allow astronauts to use the ammonium ions naturally secreted by humans [28] as a potential source for the rocket fuel's oxidizing agent. Another option that could be utilized for fuel production during future missions to Mars is iron (II) oxide

and chlorate-rich compounds present in the Martian regolith since perchlorate does not oxidize iron (II) oxide in Martian conditions at plausible timescales like chlorate substances can [29]. Nevertheless, ferrous oxide and substances such as magnesium chlorate and sodium chlorate can pose significant risks to the crewmembers' health and safety. Iron (II) oxide can spontaneously combust in the presence of air at ambient temperature (25°C) [30], while sodium chlorate and magnesium chlorate are irritants and strong oxidizers [31,32]. Although both processes represent potential options for obtaining fuel using the resources available to crewmembers on Mars, there are still many unknowns that must be considered during the missions' planning, such as the technological resources and infrastructure available for the astronauts to complete these reactions safely. Therefore, more research is necessary to investigate the viability of alternative propellant options for future crewed missions to Mars.

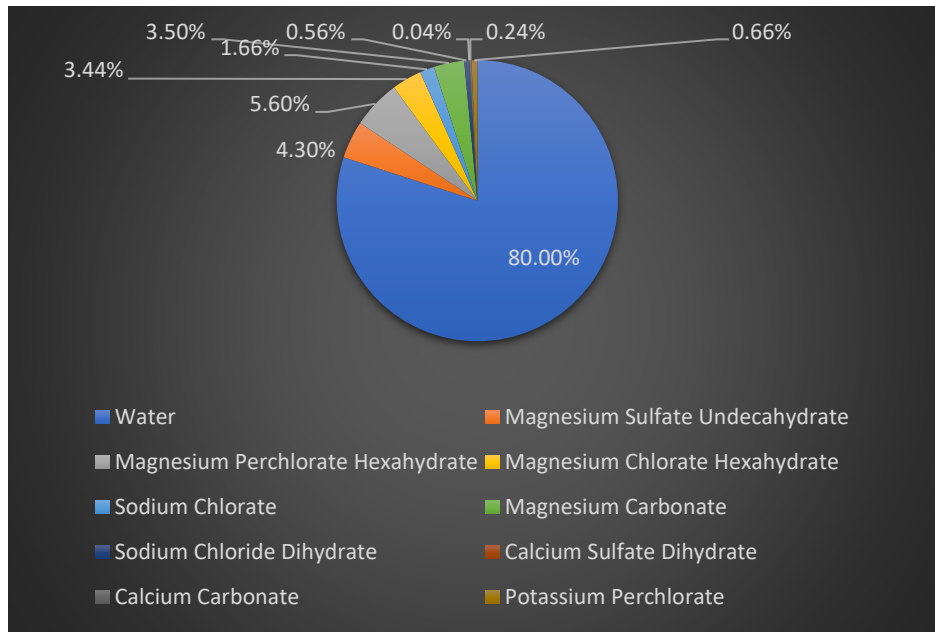
2.4. Daily Astronaut Water Needs and Subsurface Glacier Assumptions

The daily amounts of water required for a crew to survive in space has been estimated by Ewert and Stromgren's work. Essentially, for an adult crewmember that weighs 82 kg, approximately 6.47 kg is required daily plus 1.14 kg of water lost daily from the habitat [33]. Next, information from Slack et al.'s behavioral analyses involving space [34] and Mattfeld et al.'s crew time model for human space exploration [35] were used to determine that the number of astronauts on a crewed mission to Mars, for the purposes of the project's calculations, would be six. Considering this information, I calculated that the amount of water required daily for a crew comprised of six adult astronauts will be approximately 38.82 kg and that the water necessary to supply the habitat system's daily losses will be around 6.84 kg. Furthermore, using the assumption of the 4:1 mass ratio of water ice to regolith dust found inside Martian subsurface glaciers in the mid-latitudes [21,22], I also found that the amount of subsurface ice required for

the prototype to yield the necessary amount of water for a crew of six astronauts and supply their habitat system's water loss is around 48.525 kg and 8.55 kg, respectively. Finally, I utilized the regolith compositions from Toner et al.'s reanalysis of the Phoenix Lander data [18] along with the 4:1 water ice to regolith ratio [21,22] to calculate the theoretical mass percentages of each of the components of the mid-latitude subsurface ice (see Figure 2).

Figure 2

Theoretical Mass Percentage of Martian Subsurface Ice Components



Note. The mass percentages are given in $\frac{\text{Mass of Compound in kg}}{\text{Mass of Subsurface Ice in kg}}$.

2.5. Analysis of Water Purification Methods for the Prototype

To supply the water needed for future missions to Mars, I had to consider the energy and maintenance costs required in different chemical separation processes and the low temperatures and pressures found on Mars. With these criteria in mind, four procedures stood out as potential

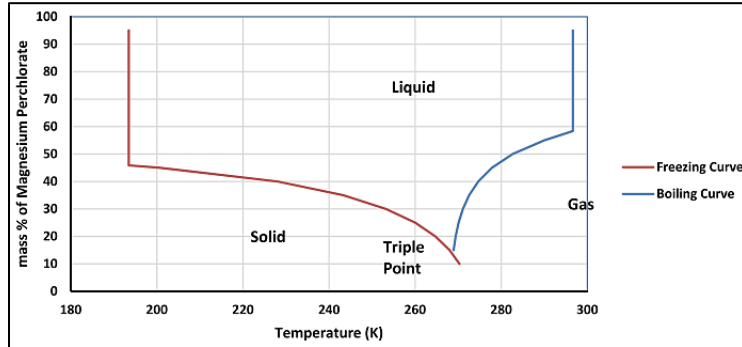
methods to obtain potable water from the frozen brine: sublimation, forward osmosis, reverse osmosis, and freeze crystallization.

2.5.1. Sublimation

When observing the thermodynamic analysis of perchlorate brine in Mars's conditions, Nair and Unnikrishnan demonstrated that if the mass percent of magnesium perchlorate in the system is below 13.5% by mass at Mars's atmospheric conditions (approximately 600 Pa) [36] (see Figure 3), sublimation becomes a viable option for the extraction of pure water from Martian subsurface ice. Hanley et al. also found that the evaporation rates and water activity increased in Martian conditions for multiple weight percentages of magnesium chlorate and sodium chlorate, which further consolidates the possibility of an evaporation reaction being a means of extracting water from subsurface ice on Mars [37] (see Figure 4). Unfortunately, there are not many data investigations involving equilibrium phase diagrams for other two-phase salt-water systems that address temperatures or atmospheric pressure levels that resemble Mars's environment and portray the systems' phase transformations into gaseous or saturated vapor forms (e.g., sublimation and evaporation). These points create opportunities for further research regarding the thermodynamic behaviors of these salts in Martian conditions. Nevertheless, because the astronauts' space habitation must replicate Earth's atmospheric pressure to ensure the crew's survival, the process would likely occur with pressure fixed at 1 atm (or 101.325 kPa). Since the latent heat of sublimation of water ice at 0°C (or 273.15 K) and 1 atm is 2,834 kJ/kg [38], the energy demand required for this process can become a significant burden on the space habitation's system, thus leading to sublimation being ruled out as a potential option to purify the subsurface ice and obtain potable water.

Figure 3

“Phase diagram of the magnesium perchlorate–water system on Mars [36]”

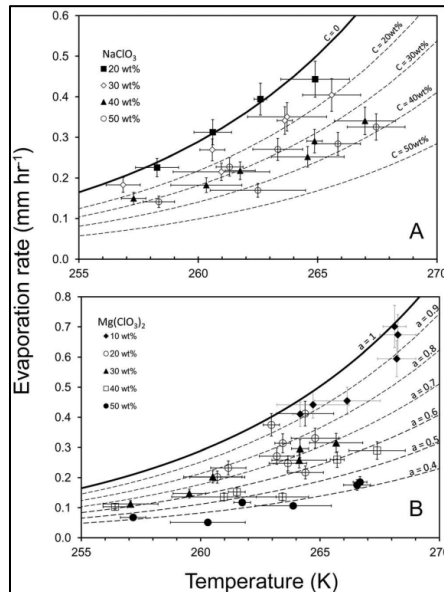


Note.

T_{eutectic} (freezing) for magnesium perchlorate was calculated to be 193.4 K at a salt concentration of 45.86 mass %. The maximum boiling point for the magnesium perchlorate–water mixture was calculated to be 296.63 K at a concentration of 58.36% by mass of magnesium perchlorate. [36]

Figure 4

“Evaporation rates of (a) NaClO_3 and (b) $\text{Mg}(\text{ClO}_3)_2$ as a function of sample temperature shown for various concentrations” [37]



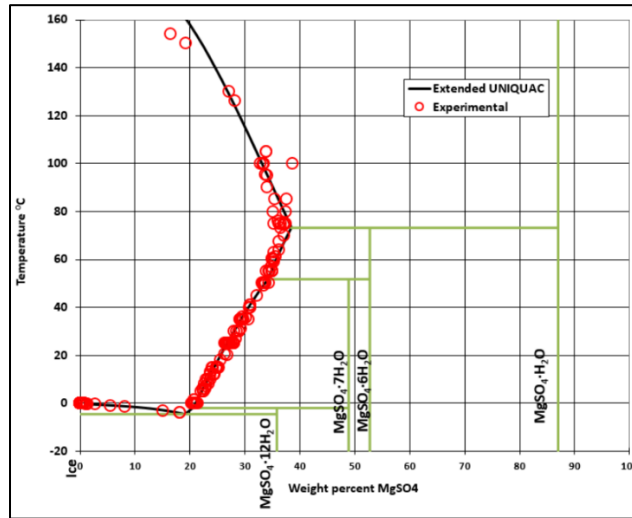
Note. “Dashed lines are theoretical evaporation rates for each concentration, calculated from a modified *Ingersoll* (1970) equation and *Pitzer* (1991) model. The solid line is for pure supercooled liquid water (*Murphy and Koop*, 2005)” [37].

2.5.2. Forward Osmosis and Reverse Osmosis

On the other hand, equilibrium phase diagrams for two-phase salt-water systems with magnesium sulfate, sodium chloride, magnesium perchlorate with a pressure fixed at 1 atm (or 101.325 kPa) indicate that these systems can exist in the liquid state [27,40] (see Figures 5, 6, and 7). Therefore, after melting the subsurface ice and removing insoluble compounds such as potassium perchlorate [18,26], calcium carbonate (calcite) [40], and magnesium carbonate [41] from the initial solution, forward osmosis or reverse osmosis can be utilized to remove the remaining perchlorate, chlorate, and sulfate salts present in the mixture. Forward osmosis is already being utilized at the International Space Station (ISS) to maintain their astronauts’ water supply in space [42], which sets a precedent for using this method to purify water in space exploration. However, for forward osmosis to occur, the selection of the concentrated solution would be crucial to allow the water to flow out of the draw solution and into the concentrated solution. Due to the high osmotic pressure of water and magnesium perchlorate’s eutectic concentration, temperature, and highly hygroscopic behavior [36,43] (see Figure 3), it is very difficult to find a two-phase solid-liquid or liquid-liquid solution that can address these criteria and ensure the process’s success.

Figure 5

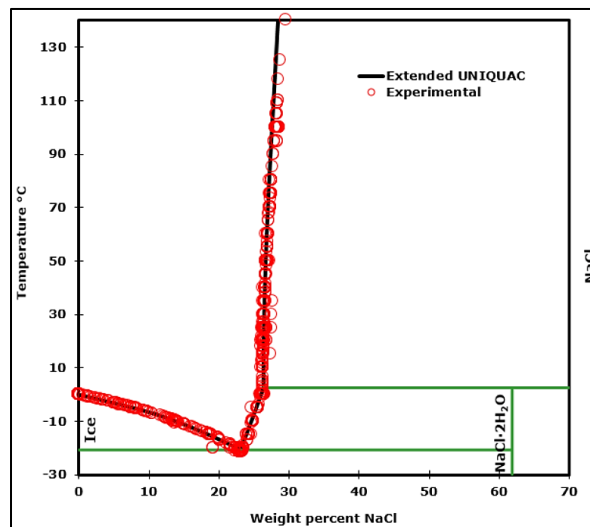
“Phase diagram for the $MgSO_4 - H_2O$ system” [39]



Note. “At temperatures above 73° , the solubility of $MgSO_4$ is decreasing. Experimental data are marked with red circles. The calculated solubility curve is marked with a black line” [39].

Figure 6

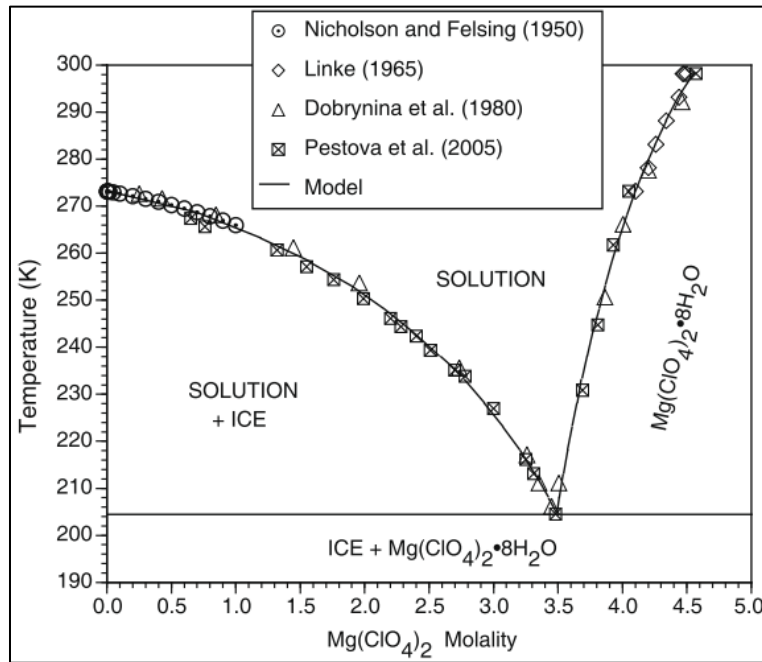
“Phase diagram for the $NaCl - H_2O$ system including an ice branch, a hydrohalite branch and a branch representing the solubility of anhydrous sodium chloride” [39]



Note. “The eutectic point is at $-21^\circ C$. The peritectic point is at $0.1^\circ C$.” [39].

Figure 7

“Equilibria for $Mg(ClO_4)_2$ solutions from 25°C to the eutectic” [26]



Note. “Symbols are experimental data; lines are model estimations” [26].

With reverse osmosis, the concerns for the process’s eligibility become the energy demands required to obtain the temperature and pressure for the treatment’s success and the concentrations of the diluted salts in the station’s dilute solution. Since the solvent flow depends on the pressure gradient and the solute gradient depends on the concentration gradient according to Fick’s Law, water flow through a semipermeable membrane will increase as the pressure is increased, with the salt flow remaining constant [44]. However, at a constantly applied pressure, the quality of the water being produced by the system will decrease as the feed’s solute concentration increases [44]. The potential variability of the diluted salts’ concentrations in the Martian glaciers due to geological and chemical phenomena on Mars’s surface over the centuries further increases the importance of determining the specific semipermeable membrane, temperatures, osmotic pressures, and energy required for the process’s success. Thus, these

constraints must be considered when evaluating the viability of reverse osmosis as part of the water treatment processes needed to ensure the survival of a space crew on Mars during longer space missions. Nonetheless, for the purposes of providing an initial water source for the astronauts while requiring the least amount of energy to sustain the process, both forward and reverse osmosis require large amounts of energy to heat up the water to room temperature (which is approximately 25°C or 298.15 K) after melting because water's specific heat capacity oscillates between 4.211 kJ/kg·K and 4.179 kJ/kg·K as the temperature increases from 275 K to 300 K [45]. In light of the energy demands required to increase the water's temperature for reverse or forward osmosis to occur, both water purification methods cannot be considered.

2.5.3. Freeze Crystallization and Progressive Freeze Concentration

The last water purification method that this literature review will consider is freeze crystallization, which separates water from a mother solution by crystallizing it into ice [46]. This process has numerous variations when other variables, such as eutectic concentrations, are considered [47], but the one this study will focus on is called progressive freeze concentration (PFC). PFC produces a large single ice crystal with high purity on a cool surface, facilitating the separation between the concentrated saline liquid and water [47]. Although PFC's productivity is slightly lower when compared to suspension freeze concentration (SFC), the water ice's purity is significantly higher than that of SFC and has a low maintenance cost [47]. Furthermore, the energy demand required for the process to occur is significantly lower because water's latent heat of fusion at 1 atm and 0°C is 333.4 kJ/kg, and the substance's specific heat capacity at -70°C (or 203.15 K) at 1 atm is between 1.66 kJ/kg·K and 1.52 kJ/kg·K [38]. Another factor that reduces the process's energy demand is that Mars's atmospheric temperature closely resembles the sublimation temperature of dry ice, indicating that the process makes use of the Martian

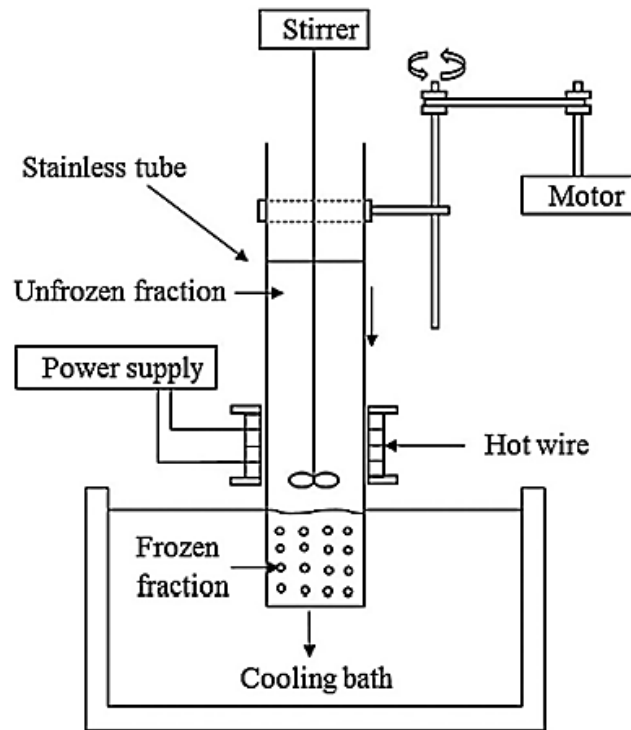
environment in extraplanetary conditions and could be simulated on Earth using a dry ice box. Since freeze crystallization satisfies the energy effectiveness and low maintenance cost criteria for the prototype, this will be the process that the research will focus on.

A PFC treatment unit usually contains the following components: a cooling bath or chiller [47,48,49,50,51], a stainless-steel tube [47,48,49,50], a hot wire with its respective power supply [47,48], salinity and temperature sensors [50], and a stirrer with its respective motor [47,48,49,50,51] (see Figure 8 for an example of a PFC system). To lower the maintenance cost while maintaining the process's efficiency, the stirrer can be substituted by a thermoelectric cooling system to use natural convection as a solution mixing mechanism. This choice will remove the need for the generator to be washed between uses and will maintain the method's productivity if the distance between the radiation tip and the freezing interface is decreased [47]. Due to the low temperatures present in the Martian atmosphere, the operational components that would contribute to the operating energy demand are salinity and temperature monitors, prototype maintenance, and thermal regulation mechanisms to compensate for significant changes in atmospheric conditions. These observations indicate that the overall operating cost for a prototype utilizing progressive freeze concentration on Mars would be low.

In conclusion, with the existing data regarding magnesium perchlorate-water systems, Mars's low temperatures can aid in potable water production on Mars when utilizing progressive freeze concentration. Additionally, the waste products from the treatment station can also be utilized to provide resources for future crewed missions to Mars, such as the rocket propellant used for the astronauts' interplanetary transportation [9].

Figure 8

“Vertical vessel PFC system” [47]



3. Methodology

This section delineates the prototype's materials and design along with the stress analyses and heat transfer calculations used to determine its dimensional and other required properties. The experimentation procedures utilized during the study are also detailed.

3.1. Materials

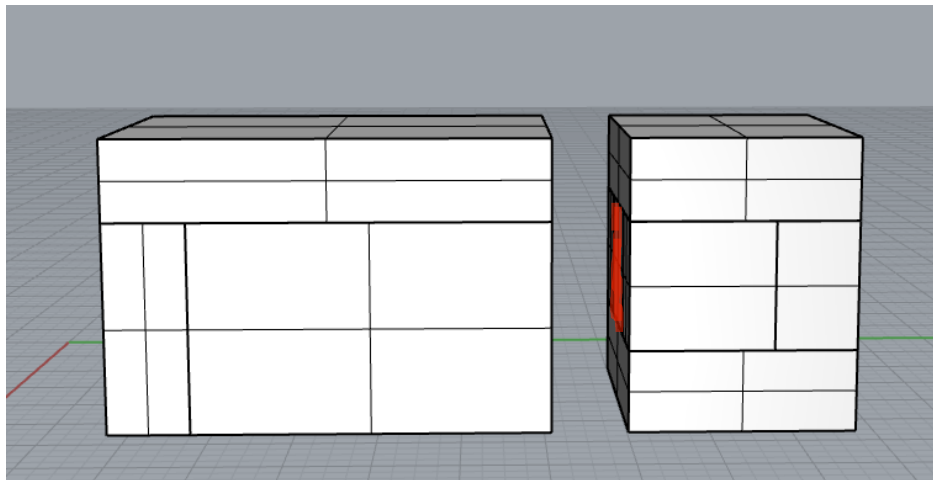
During the initial prototype version, I used a GeeBat TEC1-12706 Peltier Module to promote heat transfer within the prototype. To allow the heat transfer to occur during the experiments, Aluminum 6061 was the alloy of choice when building the cube-shaped treatment portion and the prototype's thermal interfaces due to its thermal conductivity, malleability, and cost-effectiveness. Moreover, to prepare the insulated ice box and thermally isolate the aluminum cube, an R5-rated Polystyrene Foam was used because of its low thermal conductivity and low costs. To generate a sufficient temperature differential for the progressive freeze concentration to occur, we selected dry ice as part of the prototype's ice box and heat sink mechanism due to the low temperatures at which the dry ice remains in solid form. I also used a Model 150 Orion Conductivity Meter to collect all the electrical conductivity readings for the standards, initial solutions, and resulting samples from experiments, based on the idea that the conductivity of the solution will be directly proportional to the salt's concentration since the solution only contains magnesium perchlorate salt and deionized water. Finally, when collecting data regarding the prototype's temperature throughout the experiments, the data collection setup was comprised of two Arduino Uno R3 microcontrollers, open-source Arduino Software, the serial port terminal application CoolTerm, two Adafruit Thermocouple Amplifier MAX31855 Breakout Boards, and K Thermocouples.

3.2. Prototype's Design

Before building the project's prototype, I used the principles of materials science and stress analysis to calculate the treatment station's thickness and determine its material composition (see Section 3.2.1. for more details). Moreover, I relied on the fields of heat transfer and thermodynamics to select the appropriate thickness for the prototype's insulation, find how much water ice was necessary to dissipate the heat generated by the Peltier module's hot side, and calculate the dimensions required for the ice box to contain the cooling materials (see Section 3.2.2. for more details). In the prototype's first version, Peltier module was used to obtain the temperature differential needed for progressive freeze concentration to occur within the prototype (see Figure 9).

Figure 9

Image of the Prototype's First Virtual Iteration



Note. The component on the left represents the ice box, while the component on the right is where the water would have been contained and treated. Both portions would have been held in close contact during laboratory experiments with the use of clamps. The small square highlighted

in red within the prototype's treatment station component represents the Peltier module. This image is also present in Appendix I as Figure 26.

The prototype was also separated into two components: a water ice box and a treatment station. Both components were insulated with R5-rated Polystyrene Foam and had zinc oxide thermal paste where the Peltier module interfaced with the aluminum walls to ensure thermal contact between the prototype's pieces (see Appendix I for more information on the prototype's first iteration). However, during preliminary testing, it was noted that the thermoelectric cooler couldn't sustain the required temperature differential due to insufficient heat dissipation despite the presence of an ice bath comprised of cold water and water ice. Thus, the aluminum treatment component was simply placed into the insulated ice box and a new wall and lid were made for the prototype's final version (Figure 10).

Figure 10

Image of the Prototype's Final Version



Note. This figure is also present in Appendix II as Figure 27.

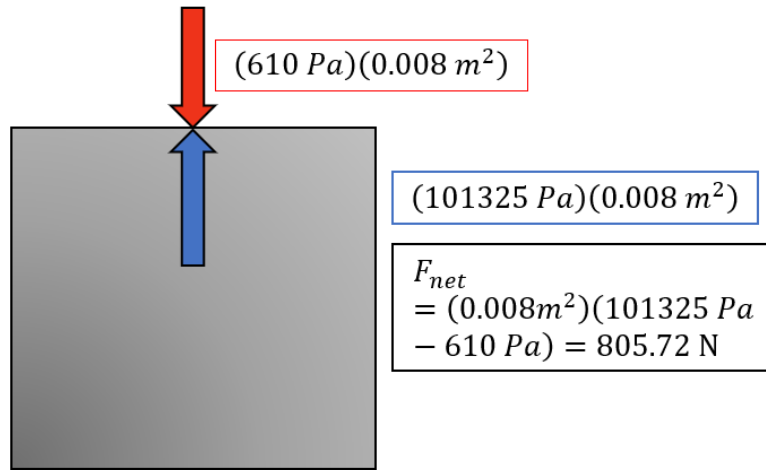
I also switched the heat-dissipating substance from a mixture of water ice and cold water to dry ice (see Appendix II for more information on the prototype's final iteration). This modification also allowed to approximate Martian atmospheric conditions due to the significant increase in carbon dioxide within the prototype and the low temperatures within the ice box, reaching -68 degrees Celsius (or 205.15 Kelvin).

3.2.1. Materials Science and Stress Analysis

Although the experiments were conducted under Earth's atmospheric conditions, the prototype should be capable of withstanding the pressure differential (see Figure 11) that would be present if the progressive freeze concentration occurred on Mars. The prototype's metallic interior will be made from Aluminum 6061 due to its high heat conductivity of approximately $180 \frac{W}{m \cdot K}$ [52], elasticity, malleability, and cost-effectiveness. Assuming that the weight of the metallic interior of the treatment station is negligible, I mapped out the forces that would be acting on that portion of the prototype using a free body diagram (see Figure 11). To calculate the force in Newtons, the Peltier module's surface area of $0.0016 m^2$ (a product of the device's length and width of 0.04 m) was used to determine the length and width of the cubic box's sides. However, since the box will not be fully sealed on top with aluminum, we will only use five sides in our total surface area calculation, thus yielding a total metallic surface area of $0.008 m^2$. After finding the device's surface area, I used the Earth's atmospheric pressure of 101325 Pa and the Martian atmospheric pressure of approximately 610 Pa at Mars's topographical datum [13] in the pressure equation ($Pressure = \frac{Force}{Area}$) to ascertain the net force acting on the box.

Figure 11

Free Body Diagram of the Prototype's Metallic Interior



Knowing the net force acting on the prototype's internal metallic structure, I searched for the Young's modulus (E) of Aluminum 6061, which is approximately 69 MPa [52], and chose a change in length that would prevent the strain from surpassing 0.01 length/length to avoid mechanical failure due to the nature stress-strain relationships. With the initial length (l_o) of the aluminum cube's face being 0.04 m and the final length (l) being 0.04001 m, it leads to the strain being equal to 0.00025 by using the following equation [52] for engineering strain (ϵ):

$$\epsilon = \frac{l - l_o}{l_o}$$

Once we know the engineering strain of the aluminum cube's side and the modulus of elasticity of Aluminum 6061, the following stress-strain equation [52] was used to calculate the engineering stress (σ) acting on each of the aluminum cube's sides is equal to approximately 0.01725 GPa.

$$\sigma = E\varepsilon$$

With the engineering strain and the net forces acting on the aluminum cube's sides, I found that the cross-sectional area (A_o) of the aluminum side was approximately $4.67 \times 10^{-5} \text{ m}^2$ using the below engineering stress equation [52]:

$$\sigma = \frac{F}{A_o} \text{ or } A_o = \frac{F}{\sigma}$$

Finally, the cross-sectional area value was divided by the aluminum side's length to find that the minimum thickness of each of the aluminum cube's walls was around 0.117 cm (or 0.046 inch). Considering this information, I selected a thickness of 0.0625 inch for the aluminum cube's walls due to manufacturing constraints.

3.2.2. Heat Transfer and Thermodynamics

When choosing the prototype's insulation material, the selection criteria were considered low thermal conductivity, high thermal resistance, and cost-effectiveness. Therefore, R5-rated Polystyrene Foam was selected for its low thermal conductivity of approximately $0.03 \frac{\text{W}}{\text{m}\cdot\text{K}}$ [53]. Next, to determine the minimum thickness required for the treatment station's insulation layer, the calculations were conducted using a modified version of Fourier's Law [54]:

$$q_x = -k A \frac{\Delta T}{L}, \text{ where}$$

q_x is the heat flux in W,

k is the material's thermal conductivity in $\frac{\text{W}}{\text{m}\cdot\text{K}}$,

A is the surface area m^2 (as mentioned in Section 3.2.1. as 0.008 m^2),

L is the thickness (m), and

ΔT is the temperature differential between outside and inside the prototype in K.

Even though the experiments were conducted under Earth's atmospheric conditions and with the prototype's outside being at room temperature, the prototype should be capable of withstanding the temperature differential that would be present if the progressive freeze concentration occurred on Mars. Moreover, the insulation's thickness must be able to maintain the temperature differential and impede excessive heat flow into the treatment station even if the Peltier module was running at low power. Thus, I used a q_x of 1 W and a ΔT of 95 K in my calculations, which returned a minimum thickness value of approximately 0.023 m (or 0.897 inch). With that information in mind, I made all the portions of the prototype's insulation layer – lids, walls, and floors – with a thickness of one inch.

After calculating the minimum thickness required for the insulation, I calculated the dimensions needed for the prototype's ice box. To describe the thermodynamic processes occurring within that component, heat exchanger modeling was used since kinetic energy, potential energy, and work were not affecting the processes within that portion of the prototype. These observations allowed me to model the ice box's internal reactions by using the following energy balance equation [55]:

$$\frac{\dot{Q}_{cv}}{\Delta h} = \dot{m}, \text{ where}$$

\dot{Q}_{cv} is the heat transfer with the surroundings in W,

Δh is the change in enthalpy in kJ/kg, and

\dot{m} is the mass flow rate in kg/s.

Considering that the Peltier module would not be running beyond 50% of its capacity within the prototype, I used 15W as my \dot{Q}_{cv} value. Furthermore, since I was using water ice when building

the prototype's first form and the ice would be thawing as heat flowed into the box through its single aluminum wall, the change in enthalpy will be equal to the enthalpy of fusion of ice (333.4 kJ/kg [38]). Using the heat exchanger equation and the previously mentioned values, the mass required for the process to occur was approximately 0.045 g/s. Considering the experiments would have a maximum duration of around one hour, the mass of ice needed for the progressive freeze concentration to succeed was around 0.162 kg (or 0.35714 lb). With this information and knowing that the density of ice is $0.9168 \frac{g}{cm^3}$ (or $0.033 \frac{lb}{in^3}$), I converted the mass of ice in pounds to cubic inches – resulting in a minimum volume of around $10.78 in^3$ – before dividing it by the aluminum interface's height and width (which is approximately 2.48 inches). These calculations revealed that the length required for the ice box to contain enough ice for one hour of experiments is around 4.35 inches.

3.3. Experimentation Procedure

Before the experiments began, I prepared initial solutions with known concentrations that would be inserted into the prototype's treatment station. For experiments 1-3, the solution was approximately 1.54 molal, while the initial brine for experiments 4-7 had a concentration of 1 molal. Test 8's initial sample had a concentration of approximately 0.89 molal, and Test 9's initial brine had a molality of around 1.01.

Three different types of tests were conducted during this stage of the project: prototype testing (experiments 1, 2, 3, 6, and 7), freezing rate testing (experiments 4 and 5), and successive testing (experiments 8 and 9). The experimentation procedures utilized in each of these experiments and their respective electrical conductivity readings will be described in the following subsections.

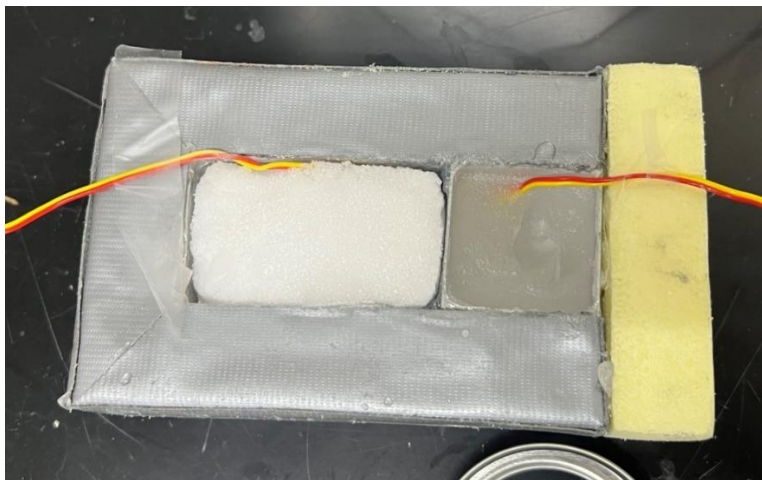
3.3.1. Prototype Testing

I prepared for the experiment by placing one thermocouple against the ice box's aluminum interface and another one alongside the treatment station's aluminum wall, specifically the one that was in direct thermal contact with the dry ice box. Once those steps were completed, the solution was inserted into the aluminum cube using a plastic syringe and sealed the top with laboratory parafilm and transparent tape to avoid any external contamination. The ice box component was filled with dry ice before being covered by the insulating lid. When the ice box's temperatures started to approach between -45 and -38 degrees Celsius, the dry ice box was refilled during the experiment. The prototype experiments lasted between 46 minutes and 1 hour and 15 minutes.

When the experiments were complete, the remaining dry ice was removed from the ice box and returned it to its cooler. Next, the remaining liquid brine was extracted from the treatment station using a syringe, leaving only the frozen aqueous solution within the prototype (see Figure 12) and placing the concentrated brine into its designated beaker or glass jar. Once the perchlorate solution had fully thawed, the liquid was collected using a different syringe and placed the sample into its designated glass container. Finally, the inside of the treatment station was cleaned using deionized water and dried before subsequent experiment or storage.

Figure 12

Experimental Setup after the Concentrated Brine's Extraction



3.3.2. Freezing Rate Testing

During the first freezing rate test – which was experiment 4 – a transparent glass jar of 1 molal solution was placed inside a refrigerator/freezer running between -7 and -7.25 degrees Celsius to test how a slower freezing rate could impact the progressive freeze concentration's outcomes. After approximately 6 hours had passed, the two-phase mixture was removed from the refrigeration unit and separated the frozen phase into a different transparent glass jar from the concentrated brine.

When performing the second freezing test – which was experiment 5 – a 100-ml glass beaker filled with one molal solution was placed inside the dry ice box to observe how a more rapid freezing rate could affect the progressive freeze concentration's outcomes. Once 24 minutes and 35 seconds had passed, the glass beaker was removed from the dry ice box due to the significant amount of frozen aqueous solution that had formed at the bottom of the recipient. Next, the remaining concentrated brine was extracted from the beaker's upper portion by pouring

the liquid into a different glass recipient. After the frozen perchlorate solution thawed, the liquid was poured into its designated glassware.

3.3.3. Successive Testing

During the successive testing trials, the transparent glass jars with the resulting less concentrated perchlorate solution and concentrated brine from experiment 5 – after collecting their electrical conductivity and molality data – were placed inside the same refrigerator/freezer that utilized during experiment 4. Once 24 hours and 10 minutes had passed since the solution's refrigeration had begun, the glass containers were removed from the freezer and the jars' frozen phases were separated into their own designated jars. Once the frozen phases had fully thawed, the electrical conductivity readings were collected.

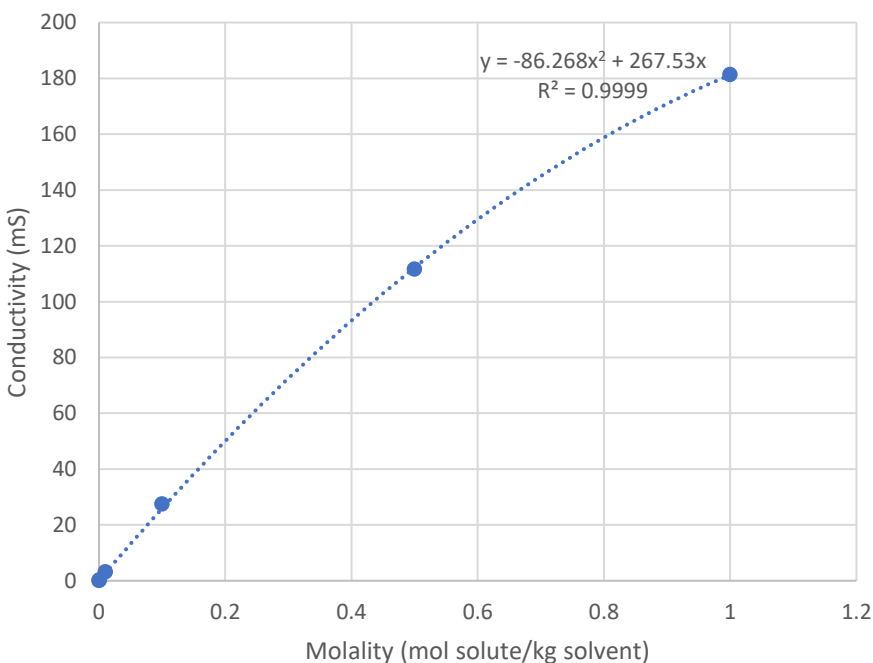
3.3.4. Electrical Conductivity Reading

When collecting the solutions' electrical conductivity data, I utilized the Model 150 Orion Conductivity Meter to measure their electrical conductivity in mS. To acquire the measurements, some solution was poured into a 50-ml glass beaker and the electrical conductivity meter's probe was inserted into the liquid. Once the reading had stabilized, I collected the data, returned the liquid to its designated container, and rinsed the electrical conductivity probe and the 50-ml beaker with deionized water between readings. However, there were situations when there was not enough brine to fully submerge the electrical conductivity meter's probe, impeding me from obtaining a reading. In those circumstances, I diluted the solution with deionized water by a factor of 3, 5, or 10, depending on the available quantity (see Section 4 for more information regarding the dilution of specific samples), before collecting the electrical conductivity data. After registering the meter's readings, I placed the diluted solution into its own glassware before rinsing the meter's probe and the 50-ml.

To adequately calibrate the electrical conductivity data, solutions with known molality were prepared – through mixing or dilution – to develop an equation and graph that represents the relationship between electrical conductivity (in mS) with respect to the aqueous solution’s molality (see Figure 13).

Figure 13

Electrical Conductivity vs. Molality Curve



Molality	Electrical Conductivity (mS)
1	181.4
0.5	111.6
0.1	27.5
0.01	3.18
0.001	0.35
0.0001	0.0374

Note. The mathematical equation that represents the previously mentioned electrochemical relationship is $y = -86.268x^2 + 267.53x$ (with a coefficient of determination – R^2 – of 0.9999), where the independent variable is the molality and the dependent variable is the electrical conductivity (in mS).

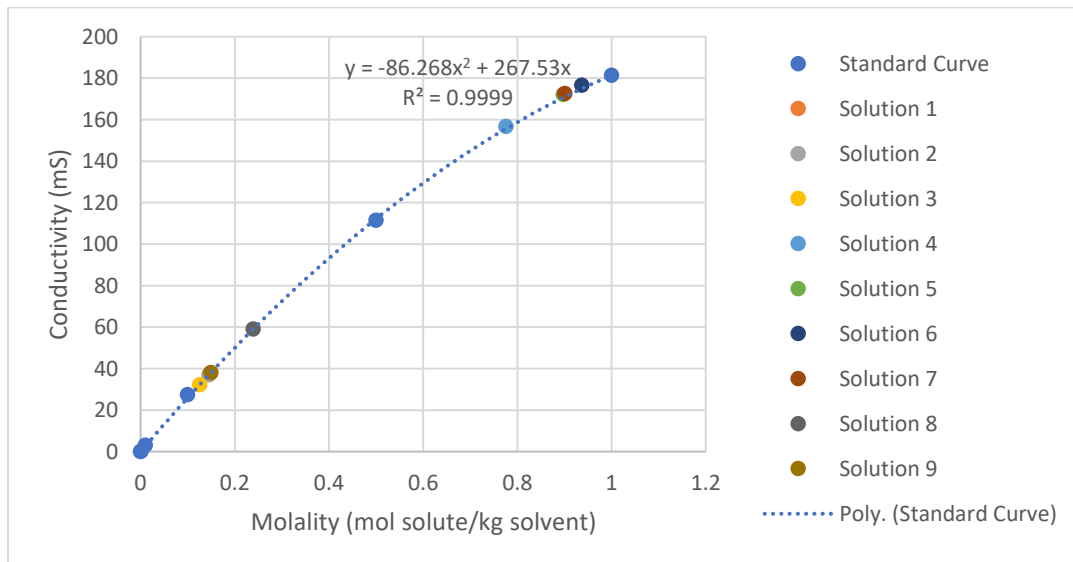
4. Results

Based on the electrical conductivity readings, all trials successfully produced a treated product of reduced salt concentration along with a residual brine of elevated salt concentration (see Figures 14 and 15 along with their respective tables for all experimental data points). The prototype trials' (experiments 1, 2, 3, 6, 7) indicated that the model's current form is functional and could be used in thawed subsurface ice purification when combined with other processes but should be improved before extraplanetary implementation.

Tests exhibited an average decrease of approximately 0.15 molal in the thawed aqueous solution's concentration compared to the initial solution's molality and a commensurate increase of approximately 0.15 molal in the concentrated brine's molality compared to the initial sample's concentration (see Figures 16 and 17).

Figure 14

Electrical Conductivity of Resulting Aqueous Solutions vs. Molality



Note. The values plotted in this figure specifically refer to the electrical conductivity readings and their corresponding molalities, but the table below displays the resulting solution's

concentrations. In this plot's corresponding data table, the asterisks refer to the dilution factors utilized during the electrical conductivity readings.

Experiment	1*	2*	3*	4	5	6	7	8**	9***
Electrical Conductivity (mS)	38	37.1	32.3	156.8	172.2	176.7	172.6	59.1	38.1
Measured Solution Molality	0.149	0.145	0.126	0.77	0.89	0.94	0.9	0.24	0.15
Final Molality	1.49	1.45	1.26	0.77	0.89	0.94	0.9	0.72	0.75
Initial Sample Concentration	1.54	1.54	1.54	1	1	1	1	0.89	1.01

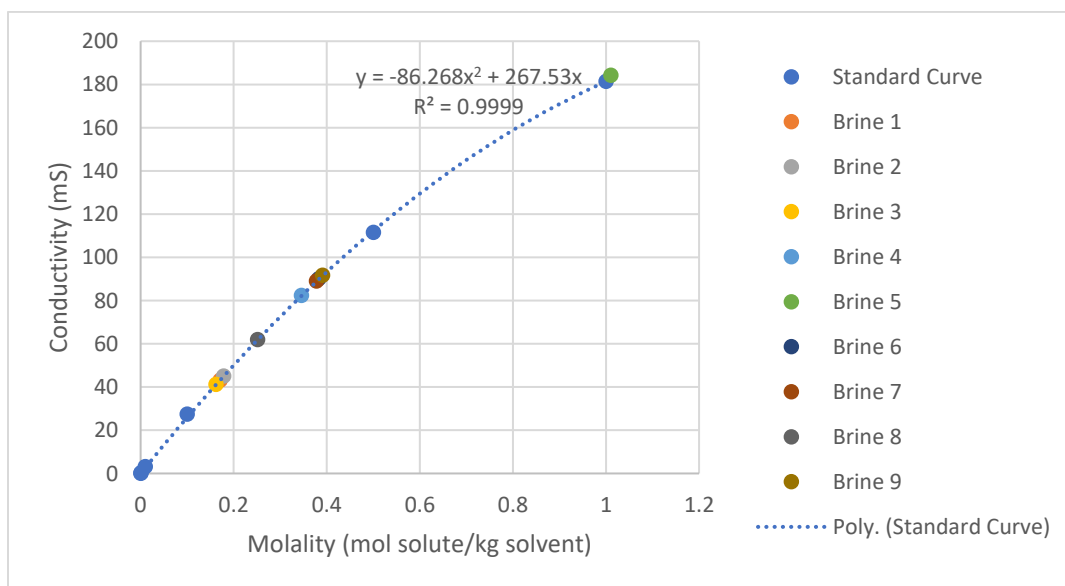
* represents the use of a dilution factor of 10

** represents the use of a dilution factor of 3

*** represents the use of a dilution factor of 5

Figure 15

Electrical Conductivity of Resulting Concentrated Brines vs. Molality



Note. The values plotted in this figure specifically refer to the conductivity readings and their corresponding molalities, but the table below displays the resulting solution's concentrations. In

this plot's corresponding data table, the asterisks refer to the dilution factors utilized during the conductivity readings.

Experiment	1*	2*	3*	4**	5	6**	7**	8***	9**
Electrical Conductivity (in mS)	43.2	45.1	41.2	82.4	184.3	90	89.1	61.9	91.7
Measured Brine Molality	0.17	0.178	0.162	0.34	1.01	0.38	0.38	0.25	0.39
Final Molality	1.7	1.78	1.62	1.03	1.01	1.15	1.14	1.25	1.17
Initial Sample Concentration	1.54	1.54	1.54	1	1	1	1	0.89	1.01

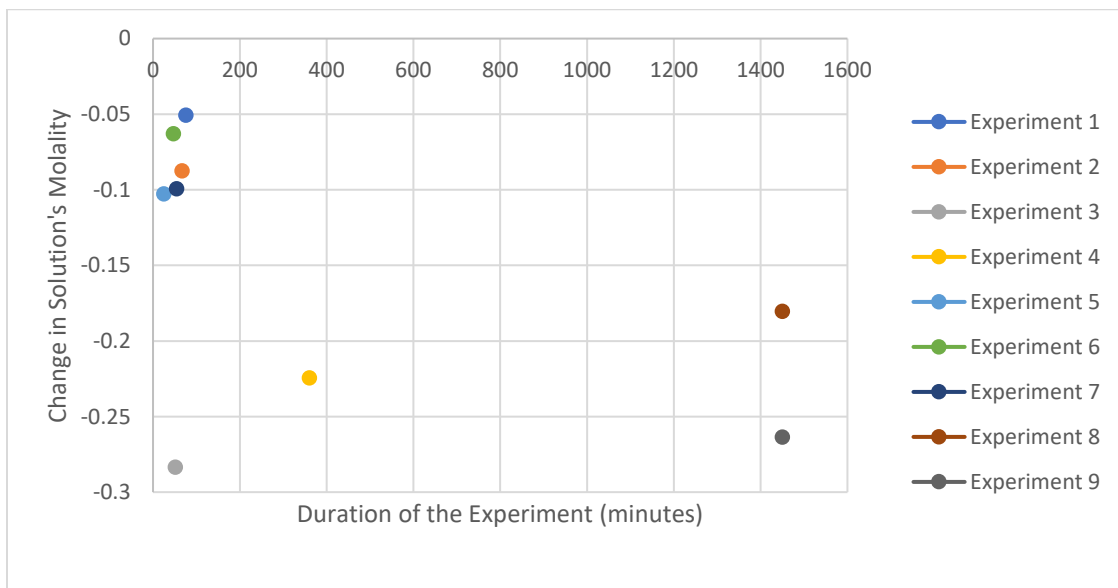
* represents the use of a dilution factor of 10

** represents the use of a dilution factor of 3

*** represents the use of a dilution factor of 5

Figure 16

Change in Solution's Molality vs. Experiment's Duration

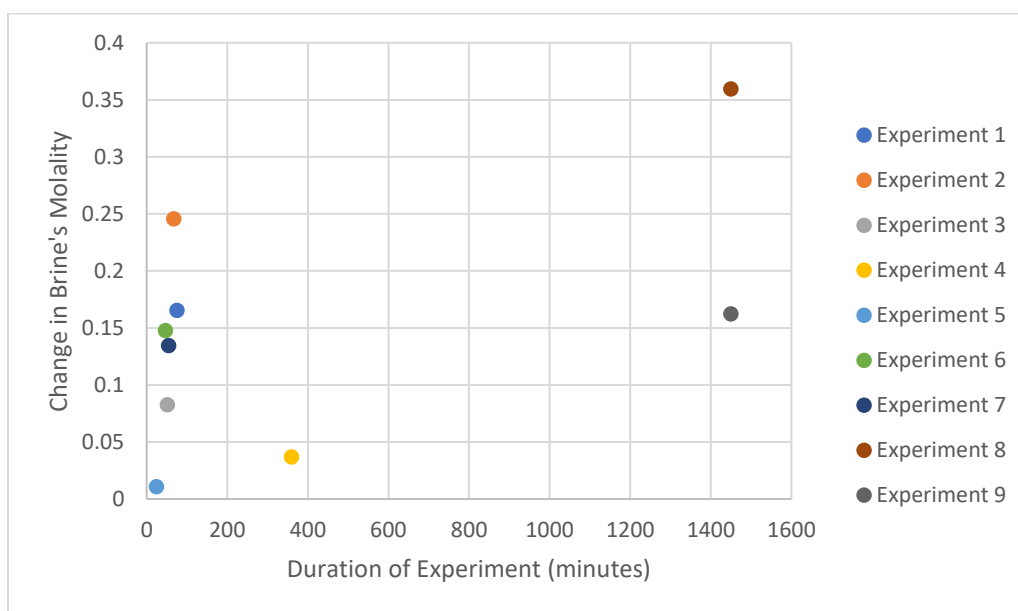


Note. This graph displays each experiment's change in the resulting thawed solution's molality (when compared to the initial sample's concentration) over time.

Experiment	Duration (minutes)	Change in Thawed Solution Molality	Change in Concentrated Brine Molality
1	75.52	-0.05	0.16
2	67.05	-0.087	0.24
3	51.42	-0.28	0.08
4	360	-0.22	0.04
5	24.58	-0.10	0.01
6	46.73	-0.06	0.15
7	54.57	-0.1	0.13
8	1450	-0.18	0.36
9	1450	-0.26	0.16

Figure 17

Change in Brine's Molality vs. Experiment's Duration



Note. This graph displays each experiment's change in the resulting concentrated brine's molality (when compared to the initial sample's concentration) over time. The information in this plot is tabulated along with the dataset from Figure 16.

I also found that experiments with slower freezing rates combined with longer experimental durations had a positive correlation with more reduced concentrations in the resulting aqueous solutions (see Figures 18, 19, 20, 21, and 22 and Appendix IV for the graphs' tabulated data). Moreover, the resulting solution's concentration was also dependent on the consistency of the low temperatures of the experiment's heat sink (see Appendix III) since it is directly associated with the experiment's cooling rate and conditions.

Figure 18

Perchlorate Concentration vs. Time (excluding the Successive Experiments – Trials 8 and 9)

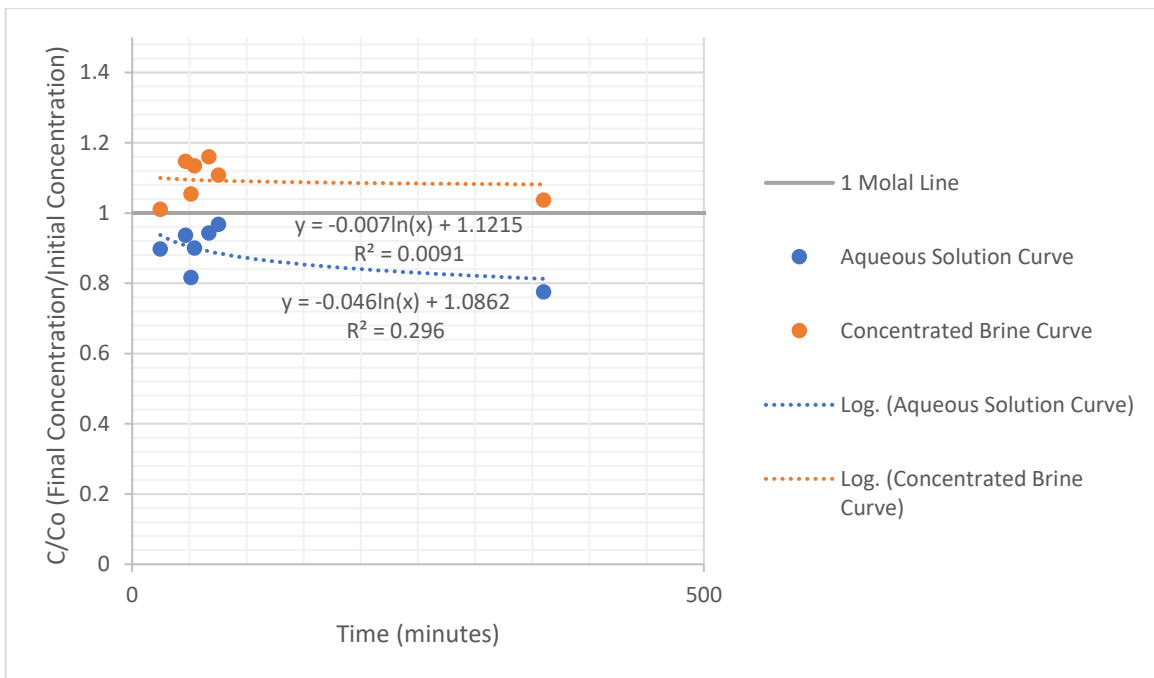


Figure 19

Perchlorate Concentration vs. Time (including the Successive Experiments – Trials 8 and 9)

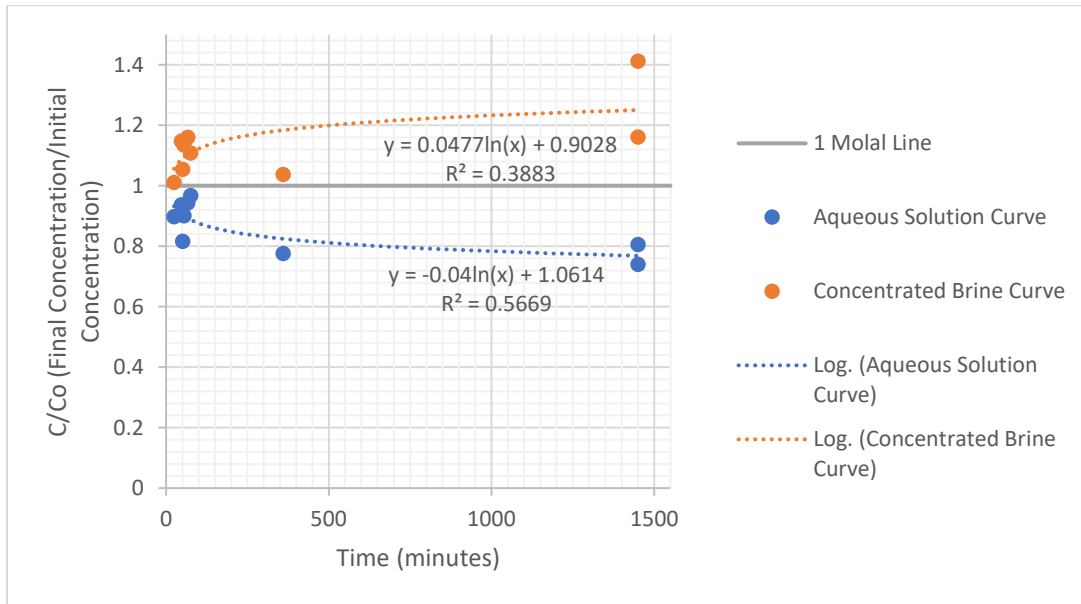


Figure 20

Final Concentration of 1-Molal Experiments vs. Cooling Rate

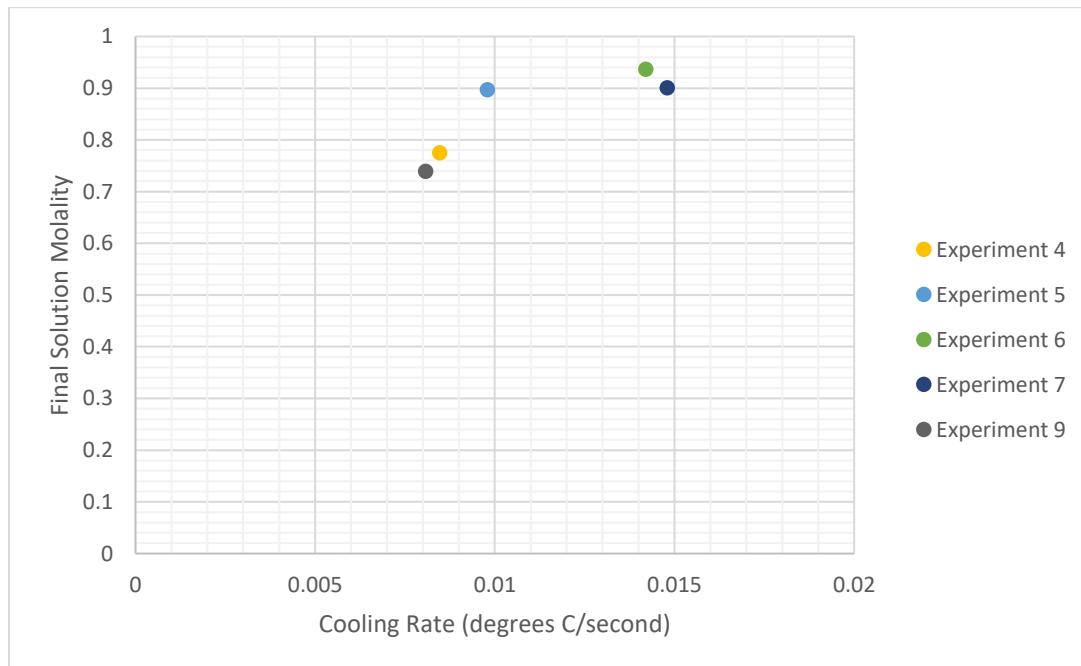


Figure 21

Final Concentration of 1.5-Molal Experiments vs. Cooling Rate

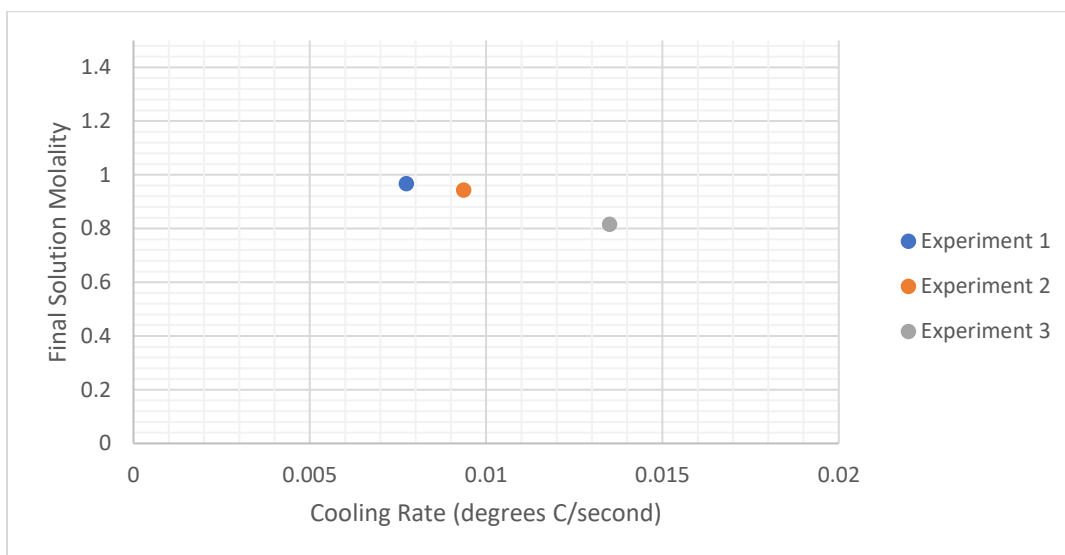
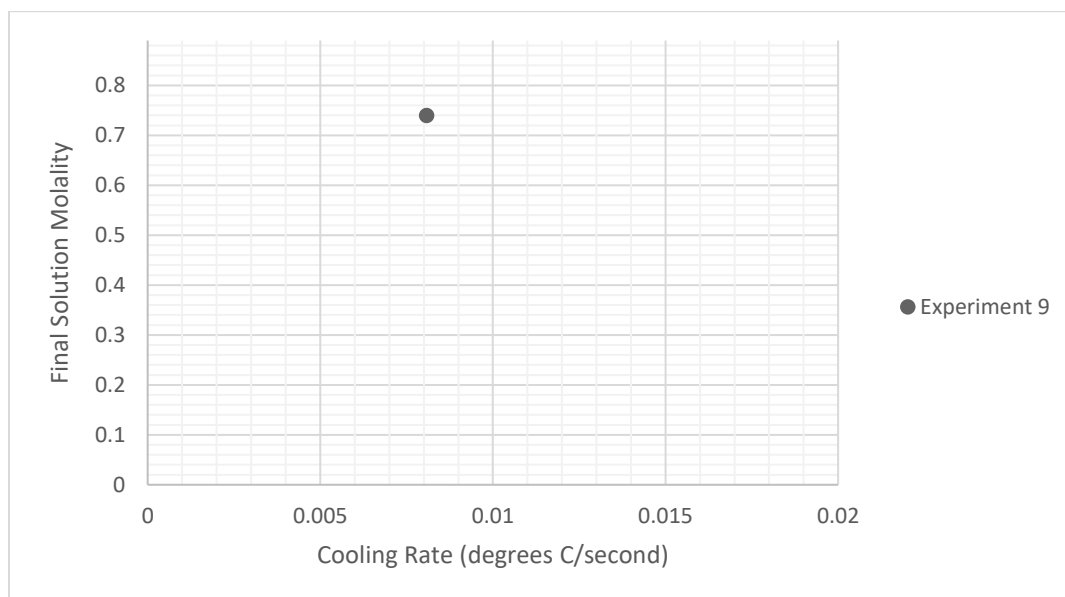


Figure 22

Final Concentration of 0.89-Molal Experiment vs. Cooling Rate

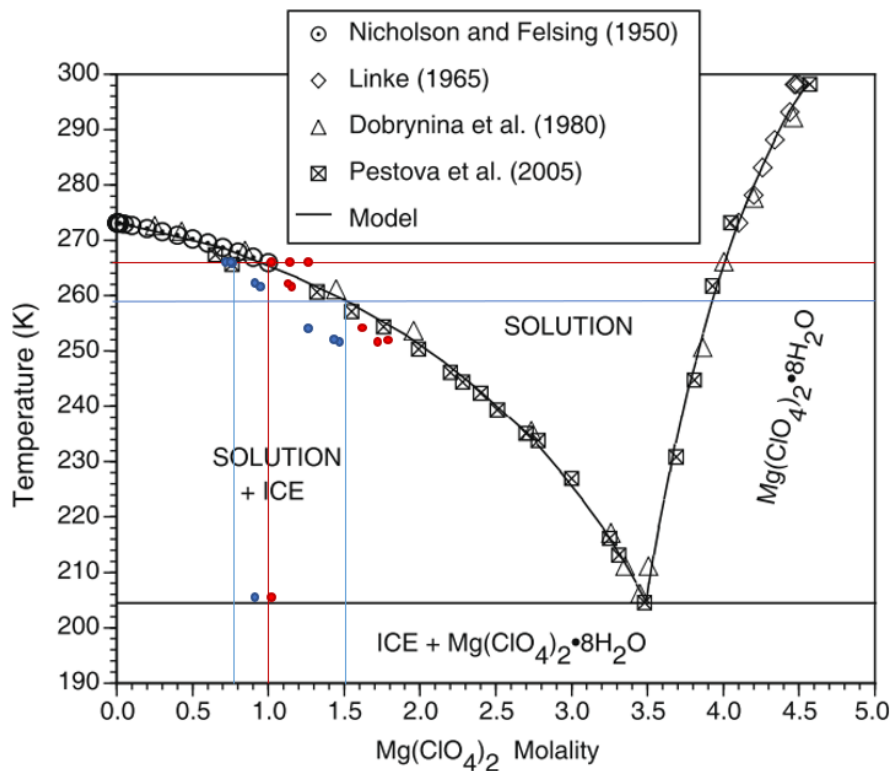


Note. This trial's initial solution was the resulting aqueous solution from Trial 5. Experiment 9 was part of the successive testing process, which consisted of trials 8 and 9.

When observing the concentration data from the trials and comparing them with the visual observations of the mass of the frozen aqueous solution, 65% to 98% of the samples' volumes were frozen during testing. However, there was a positive correlation between lesser concentrated solutions and a more substantial amount of frozen solution. Thus, combining all the observations from the previous experiments and comparing them with the data from Marion et al.'s plot (see Figure 23), I concluded that slower freezing rates, longer experimental durations, more consistent temperature control, and more substantial amounts of frozen solution caused the experimental values to approach thermodynamic equilibrium, steady-state conditions, and resulted in less concentrated magnesium perchlorate solutions.

Figure 23

Modified Equilibria Diagram for Magnesium Perchlorate solutions from Marion et al.'s "Modeling Aqueous Perchlorate Chemistries with Applications to Mars" [26]



Note. This plot is a juxtaposition of Marion et al.'s plot [26] with the data in Figures 19, 20, 21 and 22, which portrays the relationship between concentration change, cooling/freezing rate, and experimental duration. The red points represent the resulting concentrated brine molalities vs. the treatment component's temperature in Kelvin, while the blue points indicate the resulting aqueous solution molalities vs. the treatment component's temperature in Kelvin.

Finally, when analyzing the results from the successive experiments, the change in concentration was directly proportional to the number of times the progressive freeze concentration was repeated with the aqueous perchlorate solution (see Figure 16 and the data from its respective table). Nevertheless, with each time the progressive freeze concentration is repeated, less of the purified aqueous solution is available for human consumption, which must be addressed in future prototype iterations.

5. Discussion

5.1. Sources of Error

The three main sources of error that were present during the experimentation were measurement errors (specifically involving the balance, electrical conductivity meter, and pipettor), solution separation, and standard preparation due to the inherent hygroscopicity of magnesium perchlorate. The standard deviation from the balance, electrical conductivity meter, and pipettor amounted to approximately 2.71% (see Appendix V for the standard deviation calculations), indicating that the equipment and calibration solutions were reliable.

Furthermore, the progressive freeze concentration in the experiments did not occur under steady-state conditions, and the freezing process did not occur homogeneously within the less concentrated frozen portion. Due to these occurrences, brine entrapment occurred within the frozen perchlorate solution, and completely separating the concentrated brine from the frozen aqueous solution without leaving any residual concentrated brine would be difficult during the experiments. Thus, the magnesium perchlorate concentration in the frozen aqueous solution could have been smaller than the electrical conductivity measurements indicated, and the thawed solution's decrease in molality could have been more drastic than the experiments demonstrated.

One of the challenges I had to overcome during experimentation was the hygroscopicity of magnesium perchlorate since it can alter the magnesium perchlorate's mass and affect the quality of the standards and the reliability of the initial samples' molality. To determine the difference between the theoretical calculations utilizing magnesium perchlorate hexahydrate and the magnesium perchlorate hexahydrate's actual water mass values, we conducted a small experiment by heating up 6.8 grams of magnesium perchlorate hexahydrate – which was the form of magnesium perchlorate utilized during the preparation of the standards and the

experiments' initial solutions – until it became anhydrous magnesium perchlorate. After all the magnesium perchlorate hexahydrate had become anhydrous, the sample's mass dropped to 4.7 g. Comparing the theoretical mass contribution of magnesium perchlorate within the magnesium perchlorate hexahydrate

$$\frac{223.206g \text{ Mg}(\text{ClO}_4)_2}{331.30g \text{ Mg}(\text{ClO}_4)_2 \cdot 6\text{H}_2\text{O}} \cong 0.67$$

to the actual mass contribution,

$$\frac{4.7g \text{ Mg}(\text{ClO}_4)_2}{6.8g \text{ Mg}(\text{ClO}_4)_2 \cdot 6\text{H}_2\text{O}} \cong 0.69$$

I found that the actual mass values diverged from the theoretical mass values by ~2.6%.

Therefore, the theoretical values were still reliable in spite of the error.

5.2. Recommendations for Future Research and Prototype Iterations

Taking into consideration all the experimental findings, I recommend that future research and prototype iterations should use slower cooling/freezing rates, more consistent temperature control, longer process durations, and produce more substantial amounts of a frozen aqueous solution to approach thermodynamic equilibrium, steady-state conditions, and maximize the project's yields. I would also advise that future iterations of Martian water purification systems use an initial thawing station for all the Martian ice to become liquid at Earth's atmospheric pressure, decantation, filtration, 2-3 cycles of progressive freeze concentration, and the use of other purification mechanisms such as ion-exchange resin or particle activated carbon for the solutions to increase the solutions' purity until it is deemed safe and potable for the astronauts' consumption.

To adequately automate the prototype, I would suggest the addition of an electrical conductivity meter with automatic temperature correction and thermocouples within the model's

setup and connect these components to microcomputers that monitor and coordinate the process in real-time while crewmembers can collect regolith samples, rest, or perform maintenance in other portions of the space habitation.

During the prototype tests, the dry ice box's temperatures oscillated significantly whenever the container was refilled with dry ice for the progressive freeze concentration to continue. Nonetheless, this occurrence led to a faster cooling/freezing rate that decreased the quality of the resulting aqueous solutions. In light of this information, I propose removing the dry ice component in the prototype's final iteration and utilizing Mars's natural atmospheric temperature as part of the cooling process to increase the device's energy efficiency. This modification would mean that only a few heating plates or Peltier modules would be added to the device and connected to the microcomputers overseeing the water purification system's processes to ensure more consistent temperature control and steady-state conditions while progressive freeze concentration occurs.

6. Conclusions

Progressive freeze concentration was proven to be a viable option to convert frozen perchlorate brine into potable drinking water for astronauts. The study's final prototype iteration is also functional and can produce less concentrated aqueous solution. However, to increase the quality of the resulting solutions, future prototype models should incorporate the use of progressive freeze concentration combined with other processes to provide astronauts with an initial water source and to supply the crew's water losses. Adapting this project's model to the Martian environment's features and increasing its automation and energy efficiency will allow space crews to obtain water from subsurface Martian ice in the midlatitudes during their reconnaissance missions to the red planet and continue to expand our knowledge of our solar system and its past.

References

- [1] American Society of Mechanical Engineers. (12–02). *Society policy: Ethics*.
<https://www.asme.org/wwwasmeorg/media/resourcefiles/aboutasme/get%20involved/advocacy/policy-publications/p-15-7-ethics.pdf>
- [2] National Aeronautics and Space Administration. (n.d.). *Mars exploration program*. Retrieved September 16, 2021, from https://mars.nasa.gov/#mars_exploration_program/0
- [3] Withrow-Maser, S., et al. (n.d.). *Mars science helicopter: Conceptual design of the next generation of mars rotorcraft*. National Aeronautics and Space Administration.
<https://ntrs.nasa.gov/citations/20205008552>
- [4] Dixon, W., & Vogl, J. (1982). *Mars orbiter conceptual systems design study*. National Aeronautics and Space Administration. <https://ntrs.nasa.gov/citations/19830010569>
- [5] Leshin, L. A., et al. (2013). Volatile, isotope, and organic analysis of martian fines with the mars curiosity rover. *Science*, 341(6153), 1238937–1-1238937–1238939.
<https://doi.org/10.1126/science.1238937>
- [6] Hecht, M. H., et al. (2009). Detection of perchlorate and the soluble chemistry of martian soil at the phoenix lander site. *Science*, 325(5936), 64–67.
<https://doi.org/10.1126/science.1172466>
- [7] Lockheed Martin. (2019). *Mars*. <https://www.lockheedmartin.com/en-us/products/mars-base-camp.html>
- [8] SpaceX. (n.d.). *Starship*. Retrieved September 16, 2021, from <https://www.spacex.com/vehicles/starship/>

- [9] Morgan, G. A., et al. (2021). Availability of subsurface water-ice resources in the northern mid-latitudes of mars. *Nature Astronomy*, 5(3), 230–236. <https://doi.org/10.1038/s41550-020-01290-z>
- [10] Bina, A., & Osinski, G. R. (2021). Decameter-scale rimmed depressions in utopia planitia: Insight into the glacial and periglacial history of mars. *Planetary and Space Science*, 204, 1–12. <https://doi.org/10.1016/j.pss.2021.105253>
- [11] Hubbard, B. et al. (2011). Geomorphological characterisation and interpretation of a mid-latitude glacier-like form: Hellas planitia, mars. *Icarus*, 211(1), 330–346. <https://doi.org/10.1016/j.icarus.2010.10.021>
- [12] International Astronomical Union, Working Group for Planetary System Nomenclature, United States Geological Survey, & National Aeronautics and Space Administration. (n.d.-a). *Planetary names: Planitia, planitiae: Hellas planitia on mars*. Gazetteer of Planetary Nomenclature. <https://planetarynames.wr.usgs.gov/Feature/2432>
- [13] Zalewska, N. (2013). Hellas planitia as a potential site of sedimentary minerals. *Planetary and Space Science*, 78, 25–32. <https://doi.org/10.1016/j.pss.2012.12.006>
- [14] Hibbard, S. M., et al. (2021). Evidence for widespread glaciation in arcadia planitia, mars. *Icarus*, 359, 114298. <https://doi.org/10.1016/j.icarus.2020.114298>
- [15] Séjourné, A. et al. (2019). Grid mapping the northern plains of mars: Using morphotype and distribution of Ice-Related landforms to understand multiple Ice-Rich deposits in utopia planitia. *Journal of Geophysical Research: Planets*, 124(2), 483–503. <https://doi.org/10.1029/2018je005665>

- [16] Mellon, M. T., & Sizemore, H. G. (2022). The history of ground ice at jezero crater mars and other past, present, and future landing sites. *Icarus*, 371, 114667.
<https://doi.org/10.1016/j.icarus.2021.114667>
- [17] International Astronomical Union, Working Group for Planetary System Nomenclature, United States Geological Survey, & National Aeronautics and Space Administration. (n.d.-b). *Planetary names: Vastitas, vastitates: Vastitas borealis on mars*. Gazetteer of Planetary Nomenclature. <https://planetarynames.wr.usgs.gov/Feature/6333>
- [18] Toner, J. D., et al. (2014). *Soluble salts at the phoenix lander site, mars: A reanalysis of the wet chemistry laboratory data*. ScienceDirect.
<https://linkinghub.elsevier.com/retrieve/pii/S0016703714002099>
- [19] Martínez, G. M., & Renno, N. O. (2013). Water and brines on mars: Current evidence and implications for MSL. *Space Science Reviews*, 175(1–4), 29–51.
<https://doi.org/10.1007/s11214-012-9956-3>
- [20] Chevrier, V. F., et al. (2020). Global temporal and geographic stability of brines on present-day mars. *The Planetary Science Journal*, 1(3), 64. <https://doi.org/10.3847/psj/abbc14>
- [21] Boisson, J., E. Heggy, S. M. Clifford, K. Yoshikawa, A. Anglade, and P. Lognonné (2011), Radar sounding of temperate permafrost in Alaska: Analogy to the Martian midlatitude to high-latitude ice-rich terrains, *J. Geophys. Res.*, 116, E11003,
<https://doi.org/10.1029/2010je003768>
- [22] Sori, M. M., & Bramson, A. M. (2019). Water on mars, with a grain of salt: Local heat anomalies are required for basal melting of ice at the south pole today. *Geophysical Research Letters*, 46(3), 1222–1231. <https://doi.org/10.1029/2018gl080985>

- [23] United States Environmental Protection Agency. (2014). *Technical fact sheet – Perchlorate*.
https://www.epa.gov/sites/default/files/2014-03/documents/ffrrofactsheet_contaminant_perchlorate_january2014_final.pdf
- [24] Haber, L. T., et al. (2021). Impact of updated BMD modeling methods on perchlorate and chlorate assessments of human health hazard. *Toxicology Letters*, 340, 89–100.
<https://doi.org/10.1016/j.toxlet.2021.01.001>
- [25] Abernathy, C., et al. (2003). *Drinking water advisory: Consumer acceptability advice and health effects analysis on sulfate*. United States Environmental Protection Agency.
https://www.epa.gov/sites/default/files/2014-09/documents/support_cc1_sulfate_healtheffects.pdf
- [26] Marion, G., et al. (2010). Modeling aqueous perchlorate chemistries with applications to mars. *Icarus*, 207(2), 675–685. <https://doi.org/10.1016/j.icarus.2009.12.003>
- [27] Ghedjatti, I., Yuan, S., & Wang, H. (2020). Thermodynamic investigation of conventional and alternative rocket fuels for aerospace propulsion. *IOP Conference Series: Materials Science and Engineering*, 887, 012033. <https://doi.org/10.1088/1757-899x/887/1/012033>
- [28] Adeva, M. M., Souto, G., Blanco, N., & Donapetry, C. (2012). Ammonium metabolism in humans. *Metabolism*, 61(11), 1495–1511. <https://doi.org/10.1016/j.metabol.2012.07.007>
- [29] Mitra, K., & Catalano, J. G. (2019). Chlorate as a potential oxidant on mars: Rates and products of dissolved Fe(II) oxidation. *Journal of Geophysical Research: Planets*, 124(11), 2893–2916. <https://doi.org/10.1029/2019je006133>
- [30] Bretherick, L. (1990). *Bretherick's handbook of reactive chemical hazards* (4th ed.). Butterworth-Heinemann Ltd.

- [31] International Labour Organization & World Health Organization. (n.d.). *ICSC 1117: Sodium chlorate*. International Labour Organization.
https://www.ilo.org/dyn/icsc/showcard.display?p_version=2&p_card_id=1117
- [32] National Oceanic and Atmospheric Administration & Environmental Protection Agency. (n.d.). *Magnesium chlorate*. CAMEO Chemicals.
<https://cameochemicals.noaa.gov/chemical/3792>
- [33] Ewert, M. K., & Stromgren, C. (2019). *Astronaut mass balance for long duration missions*.
<https://ntrs.nasa.gov/citations/20190027563>
- [34] Slack, K. J., et al. (2016). *Risk of adverse cognitive or behavioral conditions and psychiatric disorders*. National Aeronautics and Space Administration.
<https://humanresearchroadmap.nasa.gov/evidence/reports/bmed.pdf>
- [35] Mattfeld, B., et al. (2015). *Developing a crew time model for human exploration missions to mars*. <https://ntrs.nasa.gov/citations/20150009469>
- [36] Nair, C. P. R., & Unnikrishnan, V. (2020). Stability of the liquid water phase on mars: A thermodynamic analysis considering martian atmospheric conditions and perchlorate brine solutions. *ACS Omega*, 5(16), 9391–9397.
<https://doi.org/10.1021/acsomega.0c00444>
- [37] Hanley, J., Chevrier, V. F., Berget, D. J., & Adams, R. D. (2012). Chlorate salts and solutions on mars. *Geophysical Research Letters*, 39(8), n/a.
<https://doi.org/10.1029/2012gl051239>
- [38] Haynes, W. M. (2016). *CRC handbook of chemistry and physics* (97th ed.). Amsterdam University Press.

- [39] Aqueous Solutions ApS. (2020). *Phase diagrams for binary salt solutions*.
<https://www.phasediagram.dk/phase-diagrams-for-binary-salt-solutions/>
- [40] Rau, G. H. (2008). Electrochemical splitting of calcium carbonate to increase solution alkalinity: Implications for mitigation of carbon dioxide and ocean acidity. *Environmental Science & Technology*, 42(23), 8935–8940.
<https://doi.org/10.1021/es800366q>
- [41] International Labour Organization & World Health Organization. (n.d.). *ICSC 0969: Magnesium carbonate*. International Labour Organization.
https://www.ilo.org/dyn/icsc/showcard.display?p_version=2&p_card_id=0969
- [42] Gormly, J. S., & Flynn, M. T. (2010). *Contaminated water treatment* (US7655145B1). United States Patent and Trademark Office.
<https://patents.google.com/patent/US7655145B1/en?q=+7%2c655%2c145>
- [43] O’Neil, M. J. (2001). *The merck index: An encyclopedia of chemicals, drugs, and biologicals* (13th ed.). Whitehouse Station, NJ: Merck and Co., Inc.
- [44] Montgomery, J. M. & Consulting Engineers, Inc. (1985). *Water treatment principles and design*. John Wiley & Sons.
- [45] Moran, M. J., Shapiro, H. N., Boettner, D. D., & Bailey, M. B. (2018). *Fundamentals of engineering thermodynamics* (9th ed.). Wiley.
- [46] El Kadi, K., & Janajreh, I. (2017). Desalination by freeze crystallization: An overview. *The International Journal of Thermal & Environmental Engineering*, 15, 103–110.
<https://doi.org/10.5383/ijtee.15.02.004>

- [47] Samsuri, S., et al. (2015). Review on progressive freeze concentration designs. *Chemical Engineering Communications*, 203(3), 345–363.
<https://doi.org/10.1080/00986445.2014.999050>
- [48] Rahman, M. S., et al. (2006). Freezing-Melting process and desalination: I. review of the State-of-the-Art. *Separation & Purification Reviews*, 35(2), 59–96.
<https://doi.org/10.1080/15422110600671734>
- [49] Mazli, W. N. A., et al. (2020). Study of progressive freeze concentration and eutectic freeze crystallization technique for salt recovery. *IOP Conference Series: Materials Science and Engineering*, 778, 012167. <https://doi.org/10.1088/1757-899x/778/1/012167>
- [50] Moharramzadeh, S., et al. (2021). Parametric study of the progressive freeze concentration for desalination. *Desalination*, 510, 115077. <https://doi.org/10.1016/j.desal.2021.115077>
- [51] Miyawaki, O., et al. (2012). Yield improvement in progressive freeze-concentration by partial melting of ice. *Journal of Food Engineering*, 108(3), 377–382.
<https://doi.org/10.1016/j.jfoodeng.2011.09.013>
- [52] Callister, W. D., & Rethwisch, D. G. (2018). *Materials science and engineering* (10th ed.). Wiley.
- [53] Yaws, Carl L.. (2012; 2013; 2014). Table 210. Thermal Conductivity - Building and Insulation Materials. *Yaw's Critical Property Data for Chemical Engineers and Chemists*. Knovel. Retrieved from
<https://app.knovel.com/hotlink/itble/rcid:kpYCPDCECD/id:kt00AAAHU3/yaws-critical-property/table-210-thermal-conductivity>
- [54] Lienhard, J. H., IV, & Lienhard, J. H., V. (2019). *A heat transfer textbook* (5th ed.). Phlogiston Press.

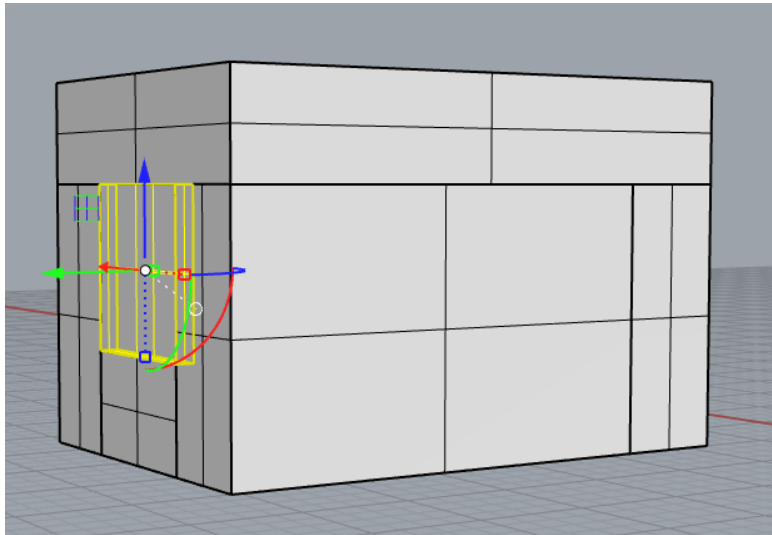
[55] Moran, M. J., Shapiro, H. N., Boettner, D. D., & Bailey, M. B. (2019). *Fundamentals of engineering thermodynamics* (9th ed.). Wiley.

Appendix I: The Prototype's First Iteration

The virtual images in this section were created using the software Rhinoceros 6 and were utilized to design the prototype's first iteration.

Figure 24

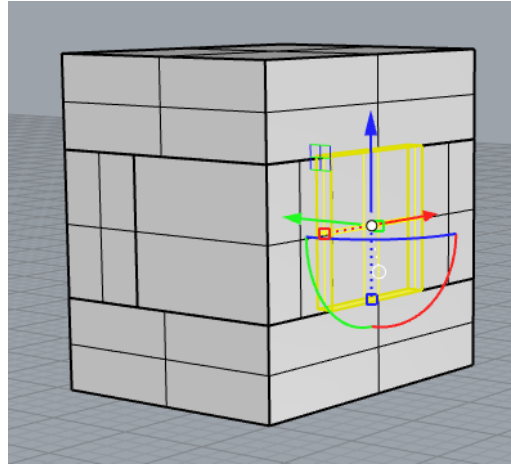
Image of the Water Ice Box



Note. The highlighted portion of this image is the ice box's aluminum interface portion, which is 1.575 in x 1.575 in x 0.0625 in. The box's inner walls are one inch thick, while the box's length is around 5.56 inches, and its width is approximately 3.81 inches. The box's walls are all 1 inch thick, and its lid's dimensions are 3.81 inches x 5.56 inches x 1 inch (approximately).

Figure 25

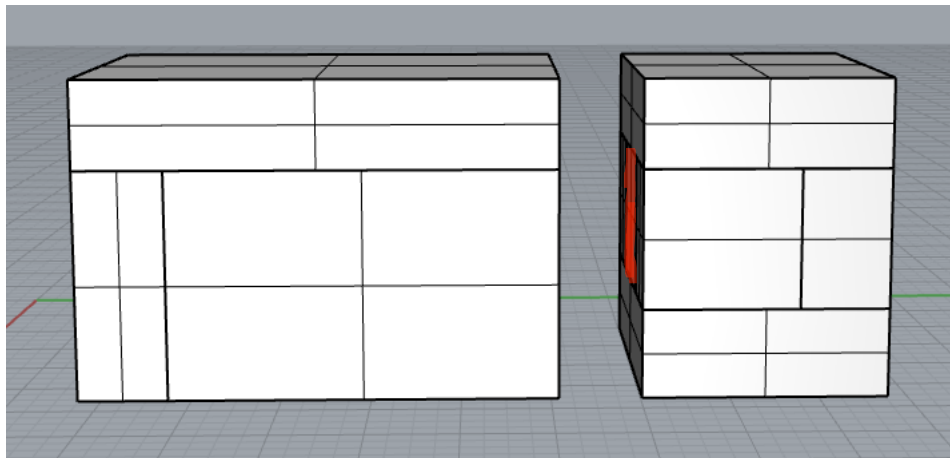
Image of the Treatment Station Component



Note. The highlighted portion of this image is the Peltier module, which is 1.575 in x 1.575 in x 0.189 in. The box's inner walls are one inch thick, while the box's length is around 2.81 inches, and its width is approximately 3.81 inches. The box's walls are all 1 inch thick, and its lid's dimensions are 3.81 inches x 2.81 inches x 1 inch (approximately).

Figure 26

Image of the Prototype's First Virtual Iteration



Note. The component on the left represents the ice box, while the component on the right is where the water would have been contained and treated. Both portions would have been held in close contact during laboratory experiments with the use of clamps. The small square highlighted in red within the prototype's treatment station component represents the Peltier module. This image is also present in Section 3.2. as Figure 9.

Appendix II: The Prototype's Final Iteration

The images in this section all illustrate the prototype's final iteration in different positions.

Figure 27

Image of the Prototype's Final Version



Note. This figure is also present in Section 3.2. as Figure 10.

Figure 28

Image of Inside the Prototype's Final Iteration



Note. The aluminum cube in this model was reused from the prototype's first iteration. Waterproof silicone sealant was used to keep the aluminum cube in place and seal off other portions of the prototype from the dry ice compartment, while the waterproof tape was used to make the inside of the dry ice portion more uniform. The prototype has around 3.81 inches in width and approximately 6.56 inches in length, while all the box's walls are 1 inch thick.

Figure 29

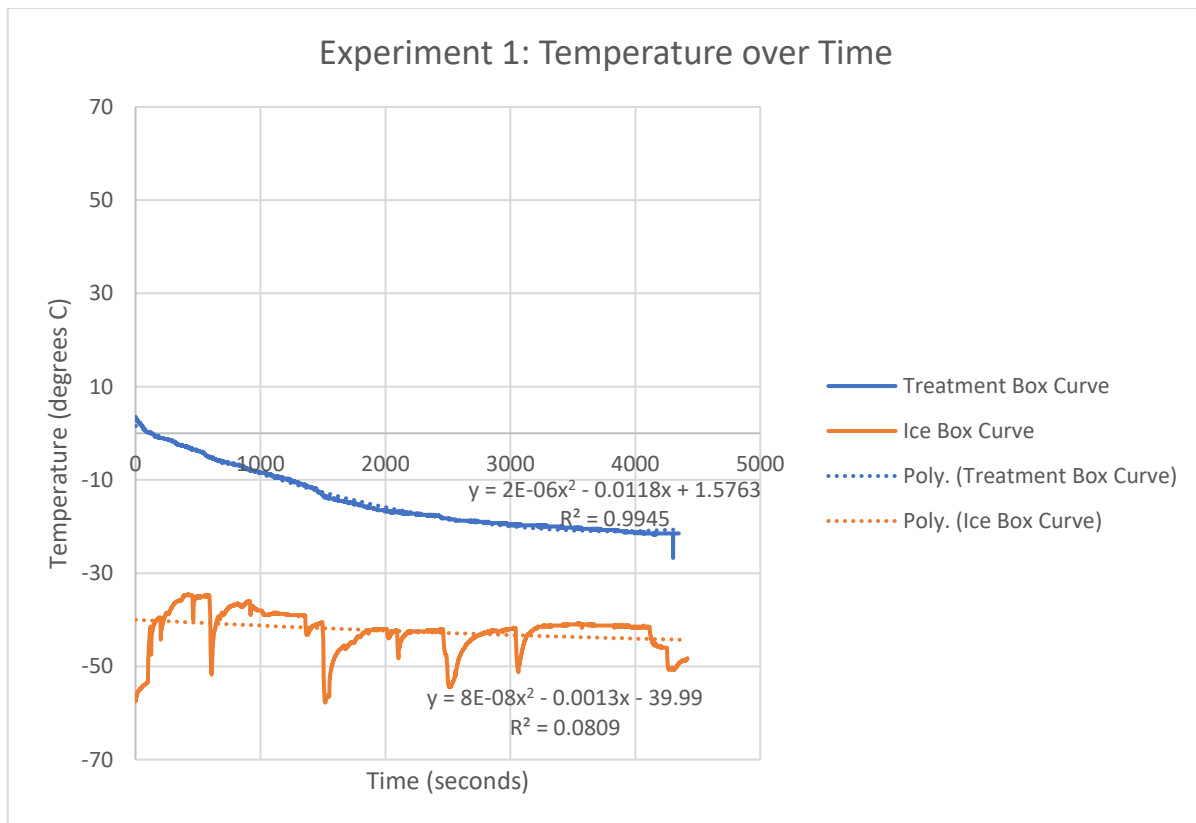
Image of the Prototype's Final Iteration while Covered



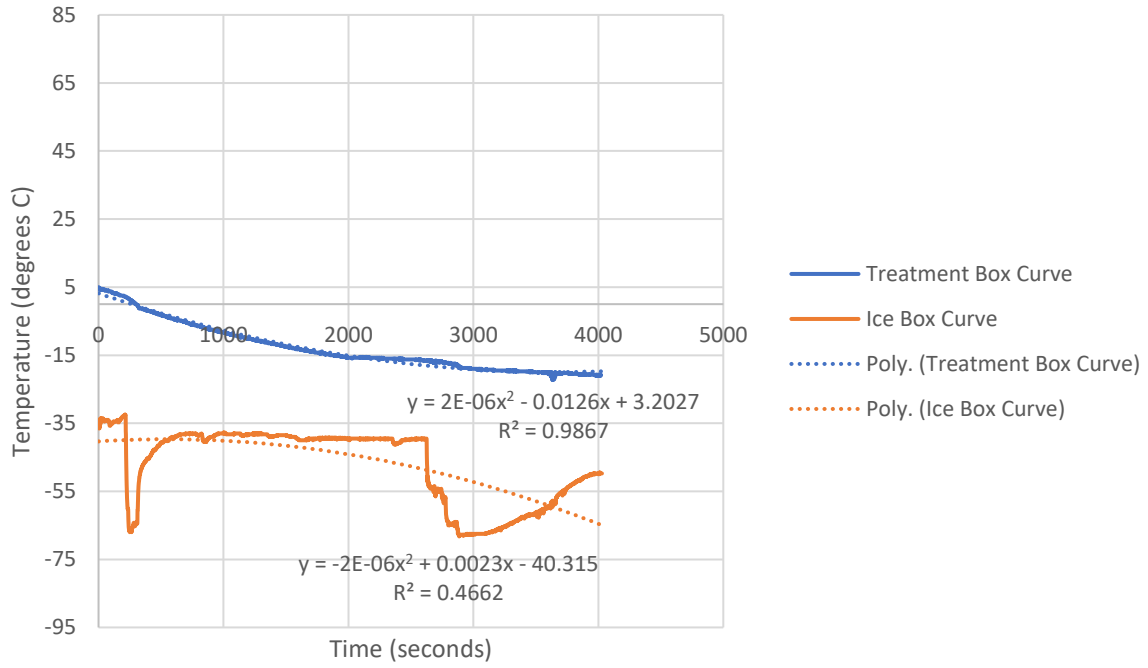
Note. The lid's dimensions are 3.81 inches x 6.56 inches x 1 inch (approximately).

Appendix III: Experimental Data involving Temperature over Time

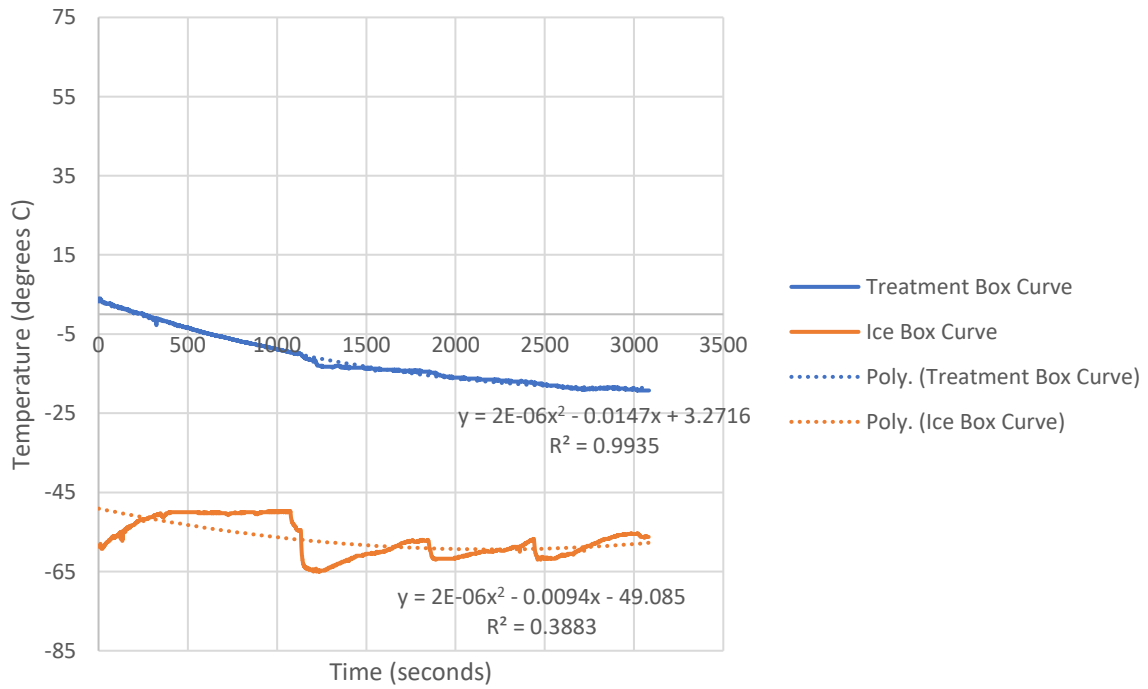
The data in this appendix was collected using the serial port terminal application CoolTerm and Arduino software, along with a thermal data collection setup consisting of two Arduino Uno R3 microcontrollers, two Adafruit Thermocouple Amplifier MAX31855 Breakout Boards, a breadboard, and Type K Thermocouples. However, since not all experiments were conducted within the prototype, only trials 1, 2, 3, 6, and 7 have plotted thermal data.



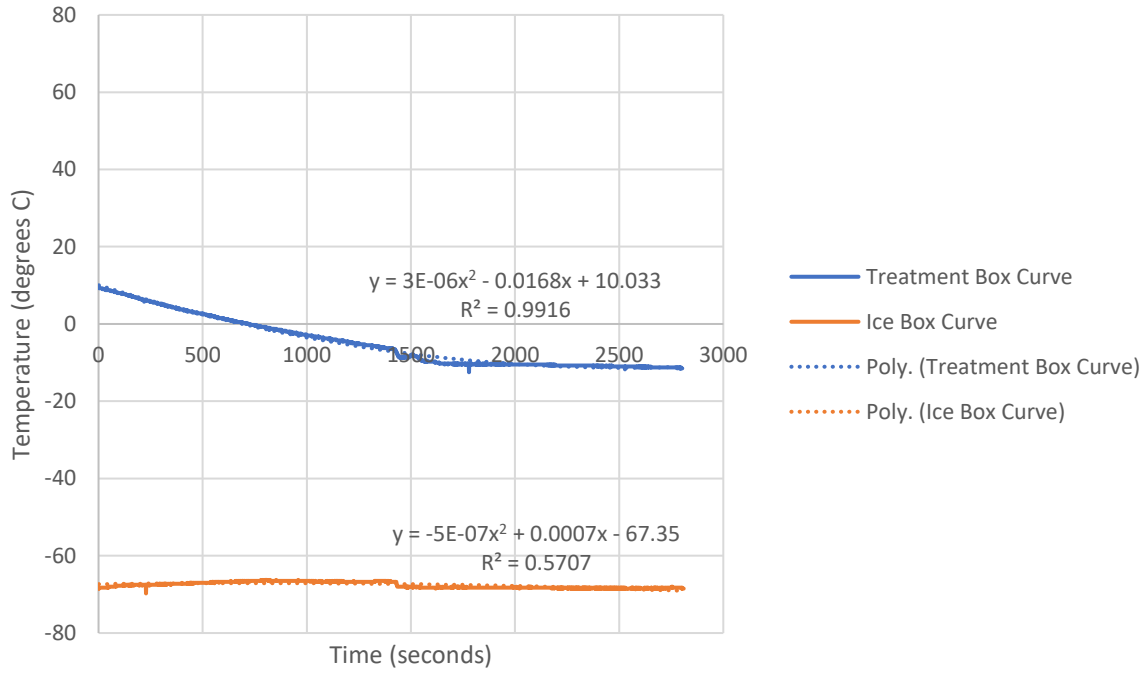
Experiment 2: Temperature over Time



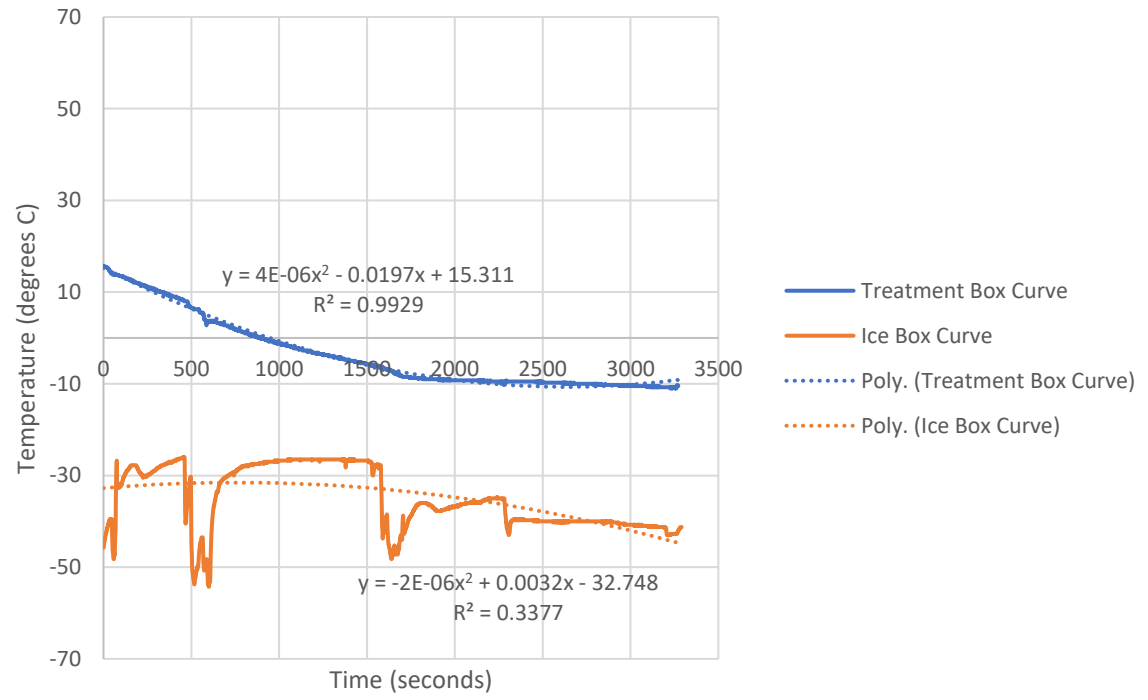
Experiment 3: Temperature over Time



Experiment 6: Temperature over Time

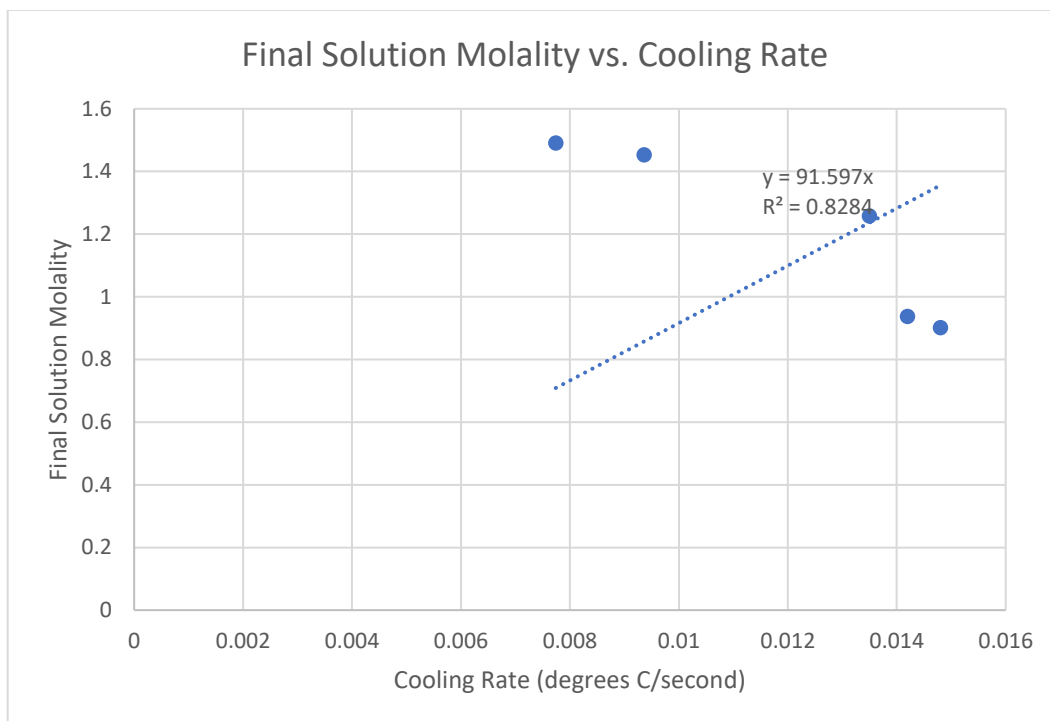


Experiment 7: Temperature over Time



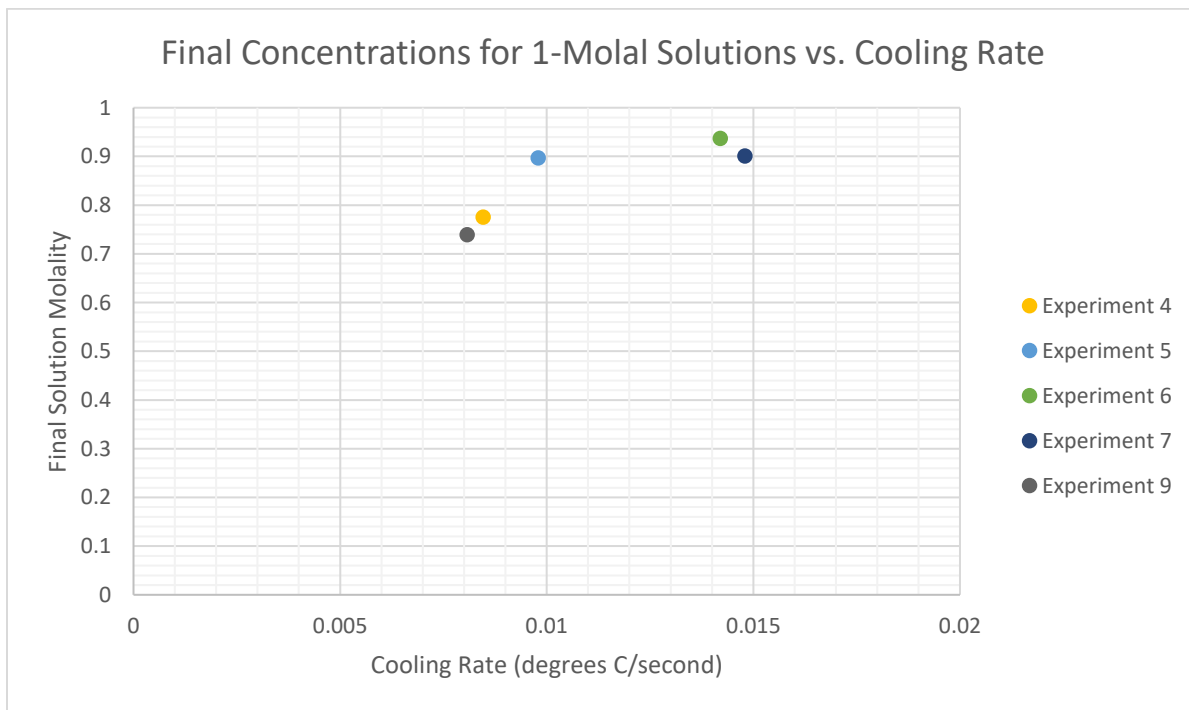
Appendix IV: Experimental Data regarding the Solution's Molality over Cooling Rate

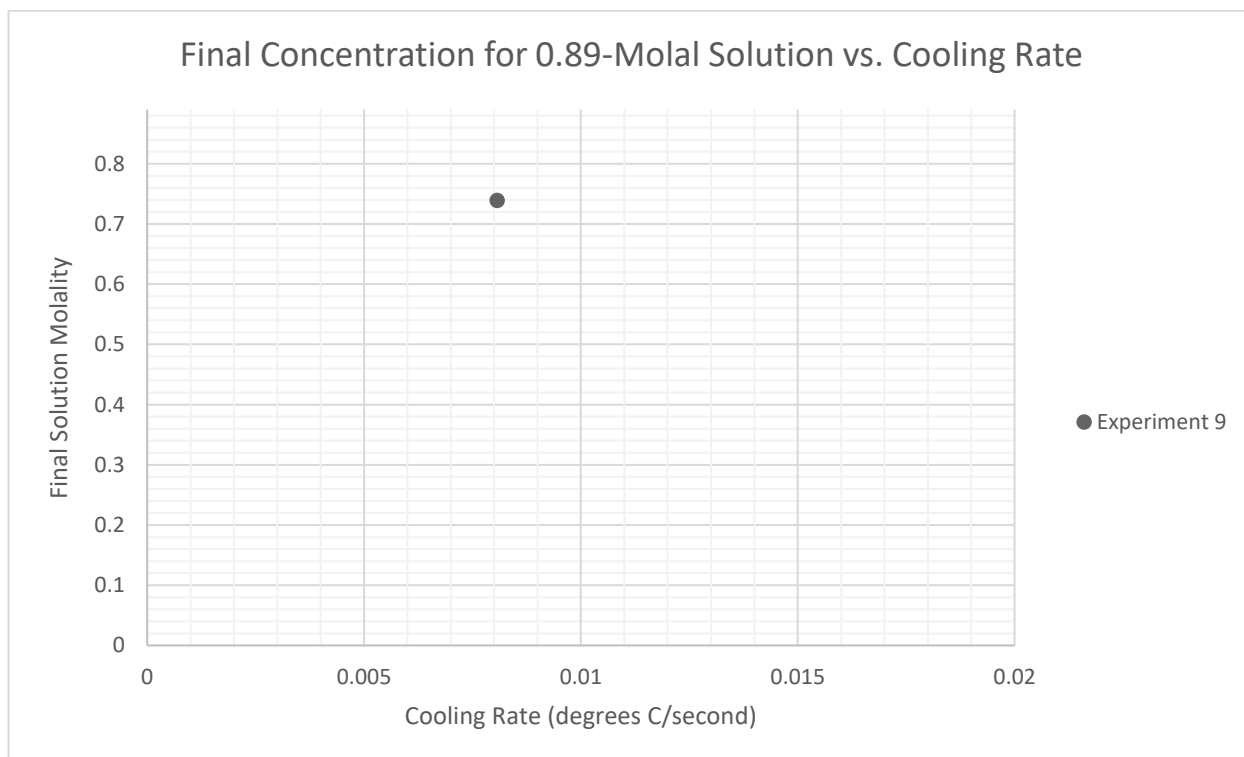
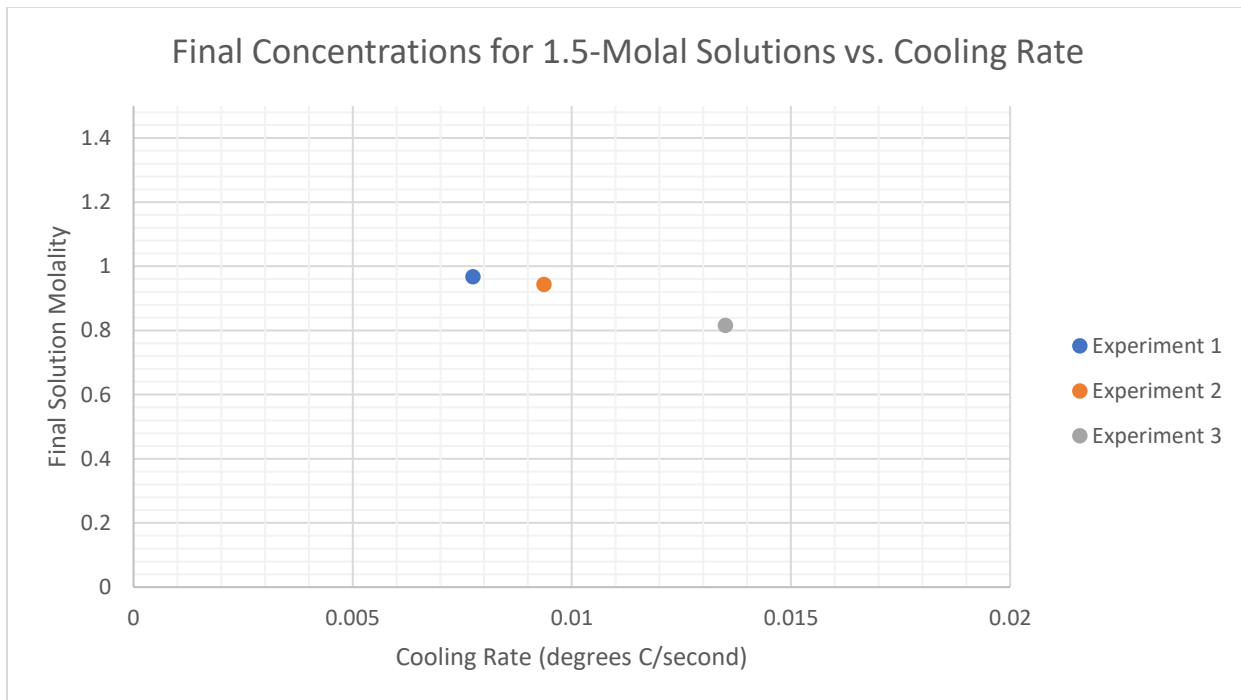
To determine the cooling/freezing rates for the experiments involving the prototype, I first selected the data from trials 1, 2, 3, 6, and 7 in which the temperatures were below 0°C and the temperature over time curve still behaved linearly. Next, the times and temperatures were used to calculate the cooling rates for those five experiments and placed into a Microsoft Excel plot to find the slope of the function that represents molality with respect to cooling rate.



Experiment	Cooling Rate (degrees C/second)	Aqueous Solution Concentration/Initial Concentration (C/Co)
1	0.0077	1.49
2	0.0094	1.453
3	0.0135	1.257
6	0.0142	0.9371
7	0.0148	0.9007

With this equation, I calculated the values for the cooling rates for the experiments that I could not collect thermal data for on Arduino (which were experiments 4, 5, 8, and 9) and created three plots relating final concentration with respect to cooling rate while using comparable datasets (experiments with solutions that started with approximately the same molality). The table below the three plots contains the information from experiments 1-9 that was used to create the graphs in Microsoft Excel.





Experiment	Cooling Rate (degrees C/second)	Final Aqueous Solution Molalities	From Arduino Data	Duration (minutes)	Duration (seconds)
1	0.0077	1.49	Yes	75.52	4531.2
2	0.0094	1.45	Yes	67.05	4023
3	0.0135	1.26	Yes	51.42	3085.2
4	0.0085	0.77	No	360	21600
5	0.0098	0.89	No	24.58	1474.8
6	0.0142	0.94	Yes	46.73	2803.8
7	0.0148	0.90	Yes	54.57	3274.2
8	0.0078	0.72	No	1450	87000
9	0.0081	0.75	No	1450	87000

Appendix V: Standard Deviation Calculations

$$\text{Standard Deviation for the Balance: } \frac{\pm 0.1g \text{ of variation}}{33.13g \text{ weighed } Mg(ClO_4)_2 \cdot 6H_2O} = \frac{0.2g}{33.13g} \cong 0.006$$

$$\text{Standard Deviation for the Automatic Pipettor: } \frac{\pm 0.1ml \text{ of variation}}{10ml \text{ solution}} = \frac{0.2ml}{10ml} \cong 0.02$$

Standard Deviation for the Electrical Conductivity Meter:

$$\frac{\pm 0.1mS \text{ of variation}}{181.4mS \text{ measured conductivity of 1 molal solution}} = \frac{0.2mS}{181.4mS} \cong 0.0011$$

$$\text{Total Standard Deviation in Decimal Form: } 0.006 + 0.02 + 0.0011 \cong 0.0271$$

$$\text{Total Standard Deviation in Percentage Form: } 0.0271 \times 100 \cong 2.71\%$$